SPECTROSCOPIC STUDIES OF III-V SEMICONDUCTOR MATERIALS FOR IMPROVED DEVICES

by

Johnny Dahl

From
Materials Research Laboratory
Department of Physics and Astronomy
University of Turku
Finland

Supervised by

Docent Pekka Laukkanen
Department of Physics and Astronomy
University of Turku
Finland

Ph.D. Mikhail Kuzmin
Ioffe Physical-Technical Institute
St. Petersburg
Russian Federation

Reviewed by

Professor Tapio Rantala
Department of Physics
Tampere University of Technology
Finland

Professor Ergo Nõmmiste
Institute of Physics
University of Tartu
Estonia

Opponent

Professor Marko Huttula
Department of Physics and Chemistry
University of Oulu
Finland

Contents

Acknowledgments

Turku, September 2014

Johnny Dahl

Abstract

Defects in semiconductor crystals and at their interfaces usually impair the properties and the performance of devices. These defects include, for example, vacancies (i.e., missing crystal atoms), interstitials (i.e., extra atoms between the host crystal sites), and impurities such as oxygen atoms. The defects can decrease (i) the rate of the radiative electron transition from the conduction band to the valence band, (ii) the amount of charge carriers, and (iii) the mobility of the electrons in the conduction band.

It is a common situation that the presence of crystal defects can be readily concluded as a decrease in the luminescence intensity or in the current flow for example. However, the identification of the harmful defects is not straightforward at all because it is challenging to characterize local defects with atomic resolution and identification. Such atomic-scale knowledge is however essential to find methods for reducing the amount of defects in energy-efficient semiconductor devices.

The defects formed in thin interface layers of semiconductors are particularly difficult to characterize due to their buried and amorphous structures. Characterization methods which are sensitive to defects often require well-defined samples with long range order. Photoelectron spectroscopy (PES) combined with photoluminescence (PL) or electrical measurements is a potential approach to elucidate the structure and defects of the interface. It is essential to combine the PES with complementary measurements of similar samples to relate the PES changes to changes in the interface defect density. Understanding of the nature of defects related to III-V materials is relevant to developing for example field-effect transistors which include a III-V channel, but research is still far from complete.

In this thesis, PES measurements are utilized in studies of various III-V compound semiconductor materials. PES is combined with photoluminescence measurements to study the SiO_2/GaAs, SiN_x/GaAs and BaO/GaAs interfaces. Also the formation of novel materials InN and photoluminescent GaAs nanoparticles are studied. Finally, the formation of Ga interstitial defects in GaAsN is elucidated by combining calculational results with PES measurements.

Tiivistelmä

Kidevirheet puolijohdekiteissä ja rajapinnoissa yleensä heikentävät laitteiden ominaisuuksia. Kidevirhe voi olla esimerkiksi vakanssi (puuttuva atomi), välisija-atomi (ylimääräinen atomi hilapaikkojen välissä) ja epäpuhtausatomi. Kidevirheet voivat alentaa (i) säteilytehoa, (ii) varauksen kuljettajien määrää ja (iii) elektronien nopeutta johtovyöllä.

On yleistä, että kidevirheiden olemassaolo voidaan päätellä esimerkiksi heikentyneestä luminesenssista tai virrankulusta. Ei kuitenkaan ole yksinkertaista tunnistaa minkälaatuisista virheistä on kyse, sillä on haastavaa karakterisoida paikallisia virheitä atomitarkkuudella. Sellainen tieto on kuitenkin välttämätöntä, että voidaan löytää menetelmiä kidevirheiden vähentämiseksi.

Kidevirheet, joita muodostuu ohuissa rajapintakerroksissa, ovat erityisen haastavia tunnistaa, sillä ne sijatsevat näytteen pinnan alla ja ovat amorfisia. Karakterisointimenetelmät, jotka ovat hyödyllisiä kidevirheiden tutkimisessa, usein vaativat hyvin järjestäytyneen näytteen. Fotoelektronispektroskopia yhdistettynä fotoluminesenssimittaukseen tai sähköisiin mittauksiin on potentiaalinen lähestymistapa rajapinnan kidevirheiden tunnistamiseen. On välttämätöntä yhdistää fotoelektronispektroskopiamittaus muihin mittausmenetelmiin, jotta muutokset spektrissä voidaan ymmärtää paremmin. Parempi ymmärrys III-V kiteisiin liittyvistä kidevirheistä on välttämätöntä III-V kanavan sisältävien transistorien kehitystyön kannalta ja paljon on vielä opittavaa.

Tässä väitöskirjatutkimuksessa fotoelektronispektroskopiaa hyödynnettiin III-V yhdistepuolijohteiden tutkimisessa. Se yhdistettiin fotolumisenssimittauksiin, kun tutkittiin SiO_2/GaAs, SiN_x/GaAs ja BaO/GaAs rajapintoja. Myös InN:n ja valoa tuottavien GaAs nanopartikkelien valmistamista tutkittiin. Lopuksi esitellään laskennallisia ja kokeellisia tuloksia Ga välisija-atomien muodostumisesta GaAsN:ssä.

List of papers

This thesis consists of five research papers. For these presented results, it was my responsibilty to perform the photoelectron spectroscopy measurements and the related data analysis. I was the principal writer for papers 1 and 3. For paper 3, I was responsible for sample preparation.

1. **J. Dahl**, V. Polojärvi, J. Salmi, P. Laukkanen and M. Guina: Properties of the SiO_2- and SiN_x-capped GaAs(100) surfaces of GaInAsN/GaAs quantum-well heterostructures studied by photoelectron spectroscopy and photoluminescence, Applied Physics Letters **99**, 102105 (2011)

2. M. Yasir, **J. Dahl**, M. Kuzmin, J. Lång, M. Tuominen, M. P. J. Punkkinen, P. Laukkanen, K. Kokko, V.-M. Korpijärvi, V. Polojärvi and M. Guina: Growth and properties of crystalline barium oxide on the GaAs(100) substrate, Applied Physics Letters **103**, 191601 (2013)

3. **J. Dahl**, M. Kuzmin, J. Adell, T. Balasubramian and P. Laukkanen: Formation of polar InN with surface Fermi level near the valence band maximum by means of ammonia nitridation, Physical Review B **86**, 245304 (2012)

4. T. Salminen, **J. Dahl**, M. Tuominen, P. Laukkanen, E. Arola and T. Niemi: Single-step fabrication of luminescent GaAs nanocrystals by pulsed laser ablation in liquids, Optical Materials Express **2**, 799 (2012)

5. P. Laukkanen, M. P. J. Punkkinen, J. Puustinen, H. Levämäki,M. Tuominen, K. Schulte, **J. Dahl**, J. Lång, H. L. Zhang, M. Kuzmin, K. Palotas, B. Johansson, L. Vitos, M. Guina and K. Kokko: Formation and destabilization of Ga interstitials in GaAsN: Experiment and theory, Physical Review B **86**, 195205 (2012)

The following papers are related to this work but are not included in this thesis.

M. Kuzmin, M. P. J. Punkkinen, P. Laukkanen, J. Lång, **J. Dahl**, L. Vitos, K. Kokko: Atomic-level understanding of interfaces in the synthesis of crystalline oxides on semiconductors: Sr- and Ba/Si(100)(2×3) reconstructions, Journal of Physical Chemistry C **118**, 1894 (2014)

P. Laukkanen, J. Lång, M. P. J. Punkkinen, M. Kuzmin, M. Tuominen, M. Yasir, **J. Dahl**, V. Tuominen, K. Kokko, V. Polojärvi, J. Salmi, V.-M. Korpijärvi, A. Ato, A. Tukiainen, M. Guina, H.-P. Hedman, R. Punkkinen: Synthesis and characterization of layered tin monoxide thin films with monocrystalline structure on III-V compound semiconductor, Advanced Materials Interfaces **1** (2014)

M. Kuzmin, M. P. J. Punkkinen, P. Laukkanen, R. Perälä, J. Lång, **J. Dahl**, J. Adell, K. Kokko: Photoemission and density functional theory study of Ge(100): Clean surface and Yb-induced (2×4) reconstruction, Surface Science **615**, 88 (2013)

M. P. J. Punkkinen, P. Laukkanen, J. Lång, M. Kuzmin, **J. Dahl**, H. L. Zhang, M. Pessa, M. Guina, L. Vitos and K. Kokko: Structure of ordered oxide on InAs(100) surface, Surface Science **606**, 1837 (2012)

M. Kuzmin, M. P. J. Punkkinen, P. Laukkanen, J. J. K. Lång, **J. Dahl**, M. Tuominen, V. Tuominen, J. Adell, T. Balasubramanian, L. Vitos, K. Kokko: Dimer-T_3 reconstructions of the Sm/Si(100)(2×3) surface studied by photoelectron spectroscopy and density functional theory calculations, Physical Review B **84**, 245322 (2011)

P. Laukkanen, J. Lång, M. Tuominen, V. Tuominen, **J. Dahl**, M. Ahola-Tuomi, M. Kuzmin, M. P. J. Punkkinen, R. Perälä, J. Adell, J. Sadowski, J. Kanski, V. Polojärvi, J. Pakarinen, M. Guina, M. Pessa, and I. J. Väyrynen: Ultrathin (1×2)-Sn layer on GaAs(100) and InAs(100) substrates: A catalyst for removal of amorphous surface oxides, Applied Physics Letters **98**, 231908 (2011)

J. J. K. Lång, P. Laukkanen, M. P. J. Punkkinen, M. Ahola-Tuomi, M. Kuzmin, V. Tuominen, **J. Dahl**, R.E. Perälä, K. Schulte, J. Adell, J. Sadowski, J. Kanski, M. Pessa, K. Kokko, B. Johansson, L. Vitos, and I. J. Väyrynen: Tin-stabilized (1×2) and (1×4) reconstructions on GaAs(100) and InAs(100) studied by scanning tunneling microscopy, photoelectron spectroscopy, and ab initio calculations, Surface Science **605**, 883 (2011)

M. P. J. Punkkinen, P. Laukkanen, J. Lång, M. Kuzmin, M. Tuominen, V. Tuominen, **J. Dahl**, M. Pessa, M. Guina, K. Kokko, J. Sadowski, B. Johansson, I. J. Väyrynen, and L. Vitos: Oxidized In-containing III-V(100) surfaces: Formation of crystalline oxide films and semiconductor-oxide interfaces, Physical Review B **83**, 195329 (2011)

M. Kuzmin, M. P. J. Punkkinen, P. Laukkanen, J. J. K. Lång, **J. Dahl**, V. Tuominen, M. Tuominen, R. E. Perälä, T. Balasubramanian, J. Adell, B. Johansson, L. Vitos, K. Kokko, and I. J. Väyrynen: Surface core-level shifts on Ge(111)c(2×8): Experiment and theory, Physical Review B **83**, 245319 (2011)

M. Kuzmin, M. P. J. Punkkinen, P. Laukkanen, R.E. Perälä, V. Tuominen, J. J. K. Lång, M. Ahola-Tuomi, **J. Dahl**, T. Balasubramanian, B. Johansson, L. Vitos and I. J. Väyrynen: Atomic structure of Yb/Si(100)(2×6): Interrelation between the silicon dimer arrangement and Si 2p photoemission line shape, Physical Review B **82**, 113302 (2010)

I have also participated in studies of catalytic materials in the following papers.

M. Stekrova, N. Kumar, A. Aho, I. Sinev, W. Grünert, **J. Dahl**, J. Roine, S. Arzumanov, P- Mäki-Arvela, D. Murzin: isomerization of α-pinene oxide using Fe-supported catalysts: Selected synthesis of campholenic aldehyde, Applied Catalysis A: General **470**, 162 (2014)

P. Mäki-Arvela, N. Kumar, S. Diaz, A. Aho, M. Tenho, J. Salonen, A.-R. Leino, K. Kordaz, P. Laukkanen, **J. Dahl**, I. Sinev, T. Salmi, D. Murzin: Isomerization of β-pinene oxide over Sn-modified zeolites, Journal of Molecular Catalysis A: Chemical **366**, 228 (2013)

1. Introduction

In the future, III-V compound-semiconductor crystals (e.g. GaAs, GaInAs, GaSb, InAs, InP) will likely become the most common materials in state-of-the-art electronics.[1] Therefore it is vital to gain a thorough insight into their properties. In particular, the development of nanoscale materials, such as nanocrystals, nanowires and nanoscale thin films, emphasizes the knowledge and control of the surface and interface properties of III-V crystals. Furthermore, semiconductor crystals are often covered by insulator films in order to prevent environment induced changes or to obtain a desired functionality of the device. The interfaces silicon forms with insulators have much lower defect densities when compared to insulator/III-V junctions in general.[2,3] III-V materials have theoretically superior charge carrier mobilities but still usually form low quality insulator/semiconductor interfaces. Since the interface quality is of the utmost importance, this has hindered the use of III-V's in microelectronic appliances.[3]

Recently, progress has been made with improving the quality of insulator/III-V junctions and the International Technology Roadmap for Semiconductors (ITRS) has recognized III-V's as a future material for semiconductor technology.[1] Moreover, there is another benefit of III-V's in comparison with traditional materials like silicon. The size of the transistors in an integrated circuit has recently shrunk to nanometer scale, and further scaling down of the transistor components is not possible because of quantum mechanical phenomena.[4] Silicon is a cheap material and will be used in the future also, at least as a substrate material, but to improve devices even further, it is necessary to search for alternative materials and III-V's are primary candidates for this aim.

III-V semiconductors are used already in a number of appliances, most notably in optoelectronics and high electron mobility transistors (HEMT) in mobile communications.[2,5] In optoelectronics III-V's have many advantages compared to silicon. Most III-V semiconductors have a direct band gap which is useful in light emitting diodes and photovoltaic cells.[6] Also, the band gap can be tuned when ternary element is introduced into the lattice.[7] This gives much flexibility when tuning the component to a certain task.

Nevertheless, the fundamental knowledge of interfaces of III-V's with other materials is still far from complete and studies of such interfaces are rather complicated. In particular, the defects of insulator/semiconductor interfaces are hard to probe because they are thin layers located beneath the sample surface and often have amorphous structure. Electrical measurements are one way to obtain information, but they have limitations, too. For example, the chemical composition of the interface cannot be studied that way. In this thesis, the author has utilized the advantages of X-ray photoelectron spectroscopy (XPS) among other techniques to elucidate interfaces and defects.

2. Basic properties of III-V compound semiconductors

The crystal structure and the electronic band structure are fundamental properties of semiconductor materials. These concepts are briefly reviewed in this chapter and their interrelation is also explained. Lastly, separate issues concerning charge carrier mobility, surface reconstructions and defects are discussed.

2.1. Crystal structure

Atoms in a crystal are not randomly distributed. They are located at well specified sites called lattice points. The lattice points form a periodic structure. To reproduce the whole crystal structure a unit cell is defined. The primitive unit cell is the smallest volume which can be periodically translated to reproduce the whole crystal structure.[8] There are two common crystal structures among III – V semiconductors with the more common one being zincblende and the other one is wurtzite.[6] Figure 1 shows these both. The lattice constants are defined as the distances between neighboring unit cells in a three-dimensional lattice. For cubic crystal structure, such as zincblende, there is only one distance to be defined: the distance between nearest-neighbor similar crystal sites. For hexagonal wurtzite structure there are two different distances: The distance between nearest-neighbour atoms in one layer and the distance between similar layers.

The chemical bonding of neighboring atoms in a III-V crystal can be described with hybrid orbitals. The valence band s^2p^1 electrons of group III atoms form new hybrid orbitals with group V atoms valence band s^2p^3 electrons. The resulting sp^3 hybrid orbitals have a tetrahedral coordination.[9] The electronic band structure will be described in detail in the next chapter.
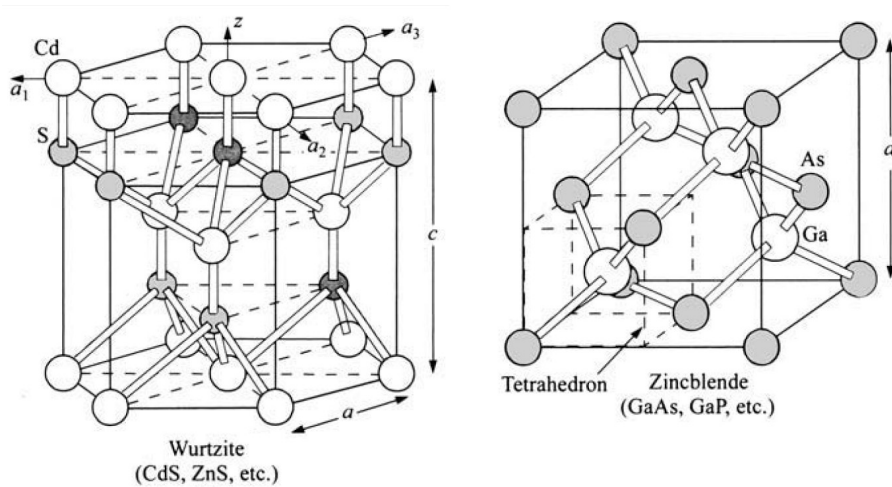

Figure 1. Wurtzite and zincblende crystal structures. Lattice constants a and c are shown. Figure is adapted from ref. 2.

Different types of monocrystalline III-V substrates (for example, two-inch GaAs and InP wafers with thickness of 0.2-1 mm) are commercially available. It is not however straightforward to build advanced devices from pure substrate crystals. In contrast, many devices contain a stack of III-V thin films. The film stacks are often produced by epitaxial growth methods like molecular beam epitaxy (MBE) [10].When growing such layered materials, the difference of the lattice constants of the film and the substrate is important. Too large lattice mismatch prevents proper growth. This is because the mismatch causes either tensile strain, when the growing material has smaller lattice constant than substrate, or compressive strain with larger lattice constant of the growing material. The strain (and the related energy) accumulates with increasing the film thickness and when the strain becomes too large dislocations will be introduced.[11] At such a critical thickness, the energy related to the dislocation formation becomes smaller than the energy gain due to the strain relief. Dislocations worsen the electrical properties of devices. Figure 2 shows dislocations in a SiGe/Si interface induced by compressive strain.
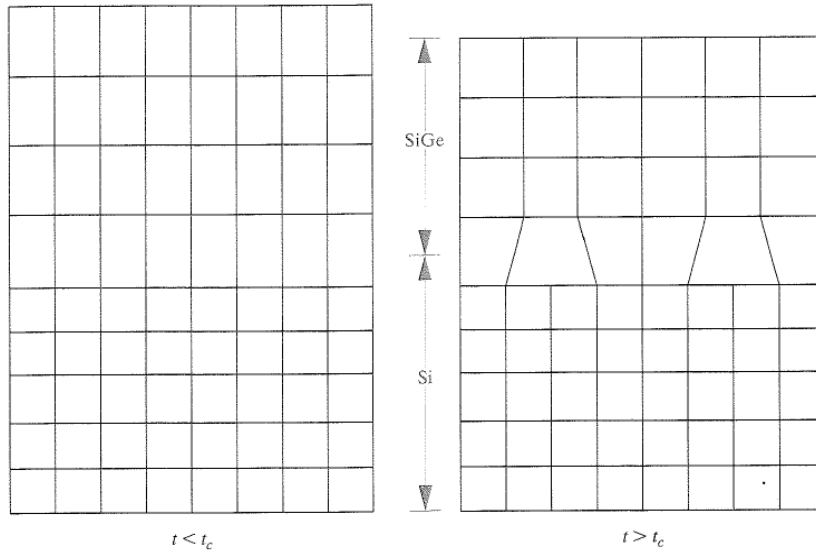
Figure 2. Dislocations induced by lattice mismatch. Figure is taken from ref 12.

Lattice constant and band gap of a particular III-V material can be tuned by introducing a third, fourth, or fifth group-III or group-V element into the crystal.[10] This is often called band-gap engineering. For example, GaAs lattice constant is about 5.65 Å and for InAs it is about 6.06 Å. By adding indium to GaAs the lattice constant of the resulting $In_xGa_{1-x}As$ lattice gets larger with increasing In content. Figure 3 shows how the amount of In affects the lattice constant of $In_xGa_{1-x}As$. Thus it is possible to grow thick $In_{0.5}Ga_{0.5}As$ films lattice matched to InP substrate. Strained quantum-well film structures are also widely used. There it is crucial to avoid the relaxation of the film stack and dislocation formation.
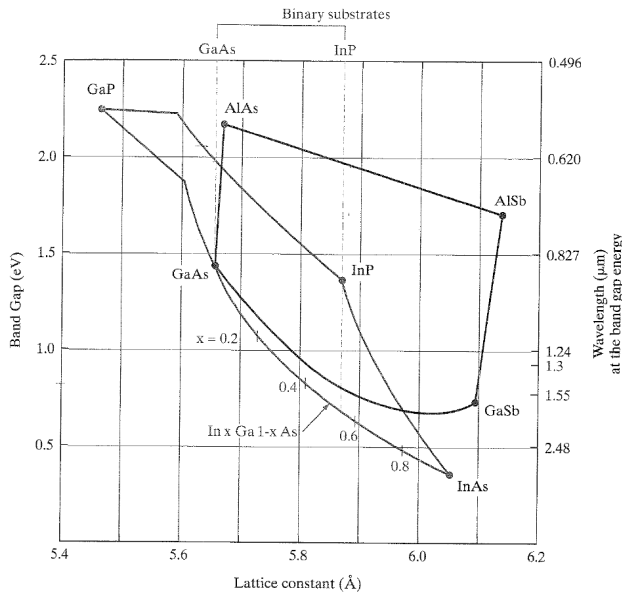
Figure 3. Bandgap and Lattice constant tuning by changing the composition of the material. Figure is taken ref 10.

2.2. Electronic band structure

The electronic band structure of a semiconductor is of paramount importance and is closely related to the crystal structure. The key properties include the width of the band gap and the effective mass of charge carriers. Figure 4 shows an energy-band diagram for GaAs. The region between the valence band and conduction band is the band gap.

All III-V semiconductors form covalent crystals with some ionic character of bonds. The group III and V atoms share their valence electrons forming sp^3 hybrid orbitals.[9,13] The overlap of hybrid orbitals gives rise to the formation of bonding and antibonding orbitals. This effectively splits the band to two different bands separated by a band gap. The bonding orbitals are filled with electrons and form the valence band (VB). The antibonding orbitals are empty at 0 K and form the conduction band (CB). The band gap between them contains no electronic states if a semiconductor is free of crystal defects (including surface states). Figure 5 shows the energy levels of sp^3 dangling bond states of GaAs.

5

Figure 4. Energy-band diagram for GaAs. Figure is taken from ref 13.
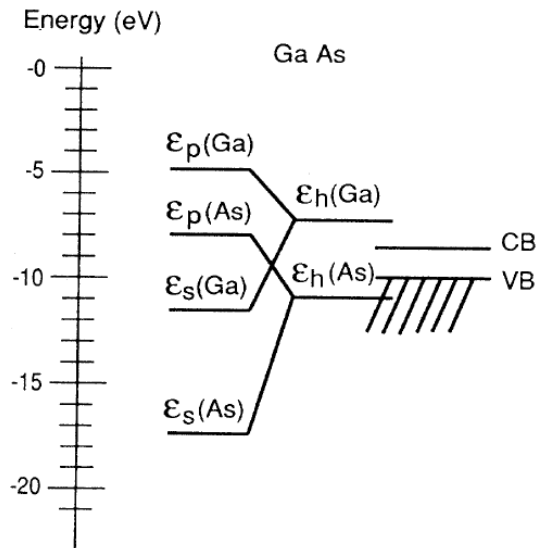
Figure 5. Energy levels of the sp^3 dangling-bond states of GaAs. Figure is adapted from ref. 14.

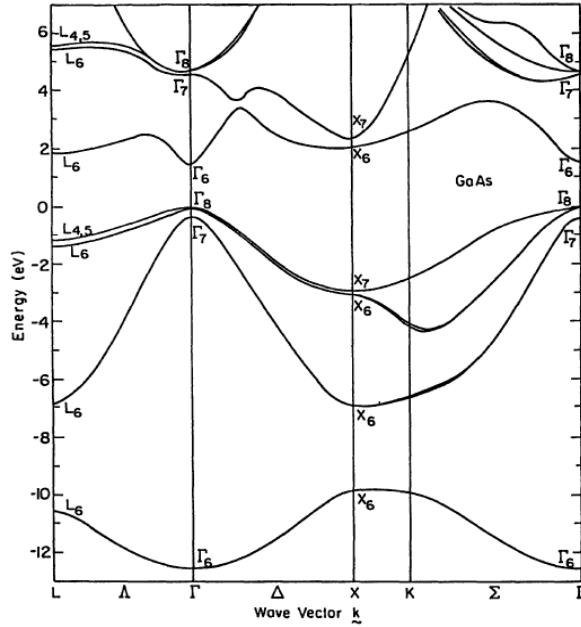Concepts related to band structure are Fermi level, work function and electron affinity. For undoped semiconductor at 0 K the Fermi level locates at midgap position. Doping will shift the Fermi level towards conduction band (n-doping) or valence band (p-doping). The work function is the energy difference of vacuum related to the Fermi level. The electron affinity denotes the energy obtained by moving an electron from vacuum to the conduction band minimum. Figure 6 shows the energy band diagrams of an n-type semiconductor and a metal and the resulting band bending when they are brought into contact. When a semiconductor surface is illuminated with sufficiently energetic photons, electrons in the valence band can be excited to the conduction band (photovoltaic effect).[15] The energy threshold for this is the width of the band gap. Moreover, the photon-excited electrons can emit from the material into a vacuum providing that the photon energy is large enough (photoelectric effect).[16]

Figure 6. Energy band diagrams and band bending. E_{vac} is the vacuum energy, E_c is the energy level of conduction band minimum, E_v is the energy level of valence band maximum, Φ_m is the metal work function, Φ_s is the semiconductor work function and χ_s is the electron affinity. Figure is taken from ref 17.

III-V compound semiconductors provide a wide range of band gaps. They vary from small band gap materials *e.g.* InSb (0.17 eV) used in infrared detectors to large *e.g.* G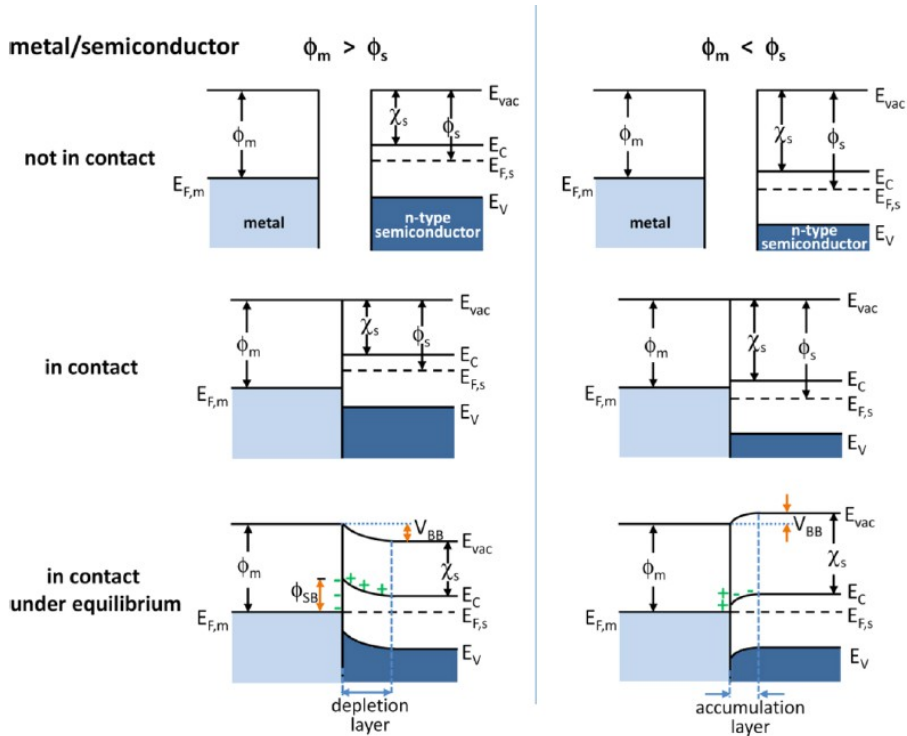aN (3.44 eV) and AlN (6.2) eV used in blue and ultraviolet LEDs and lasers.[6] The band gap can be either direct or indirect. The band gap is direct if the valence band maximum (VBM) and conduction band minimun (CBM) locate at the same electron wavevector (k), as in Fig. 4. Indirect band gap means that a phonon assisted transition in the k vector is needed for the electron to transfer from VBM to CBM (or vice versa). This lowers the probability for radiative electron transfer considerably and indirect band gap materials are not preferable to be used in light-emitting devices. Therefore silicon with indirect band gap is less useful compared to many III-V's for optoelectronic devices.[18]

Many III-V semiconductors have higher electron mobility than silicon, which means higher drift velocity for electrons in III-V's as a function of the electric field applied.[3,19-21] The mobility is affected by the effective mass of electrons, which is determined by band curvature and scattering probability. Since the electron mobility is directly proportional to the maximum possible operating frequency of a transistor, this opens up possibilities for III-V transistors. Indeed the high-frequency transistors of mobile phones are made of III-V's. Furthermore, the size of silicon transistors in integrated circuits is reaching a minimum limit beyond which the properties of Si transistors are impaired significantly.[4] Therefore alternative materials have to be found, and the III-V films are now the most potential materials to replace the Si channel in future transistors of integrated circuits. Table I and Fig. 7 show the comparison of carrier mobilities for different semiconductors at room temperature.

Table I. Electron and hole mobilities for selected semiconductors[22]

Semiconductor	Electron mobility ($cm^2V^{-1}s^{-1}$)	Hole mobility ($cm^2V^{-1}s^{-1}$)
Si	1400	450
GaAs	8500	400
InAs	40000	500
InSb	77000	850
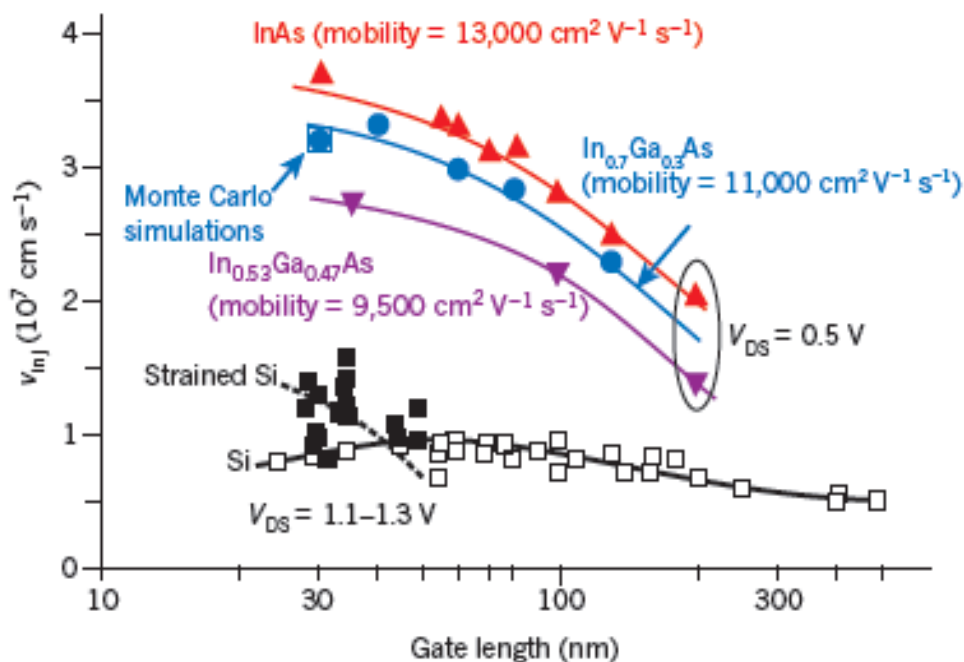
Figure 7. Comparison of electron maximum velocities and operation voltages for Si and III-V transistors shows the benefits of III-V. Figure is taken from ref 23.

2.3. Surface structure

When a surface is formed by cleaving a bulk crystal, so called dangling bonds appear at the surface. Such bonds are not energetically favorable and the surface layer can undergo a transformation called surface reconstruction. The surface reconstruction, which is defined as a change in the in-plane lattice as compared to the bulk, is common on III-V surfaces. The driving force for reconstructing is a minimization of surface free energy. This process is controlled by a complex interplay of different factors including balance between the gain in energy due to elimination of dangling bonds and the loss in energy due to introduced surface stress at the surface. The surface can also adsorb foreign atoms that become bonded to the surface via unsaturated dangling bonds. Thus, the atomic structure of semiconductor surface is usually much more complex than that of the bulk.[24] The presence of reconstructions at the III-V surfaces significantly affects the properties

of the interfaces (e.g., the compositional homogeneity) III-V surfaces form; the reconstruction serves as a template on which the new layer is grown. The reconstruction formation depends strongly on the preparation conditions on the surface. Common feature of III-V surface reconstructions is the formation of atomic pairs (dimers), which reduce the amount of energetically unfavored dangling bonds. Let's consider an example of the GaAs(100) reconstructions shown in Fig. 8. The most common reconstructions seen on the GaAs(100) are: c(4x4), (2x4), (6x6), and (4x2) with decreasing the amount of As in the surface preparation conditions.
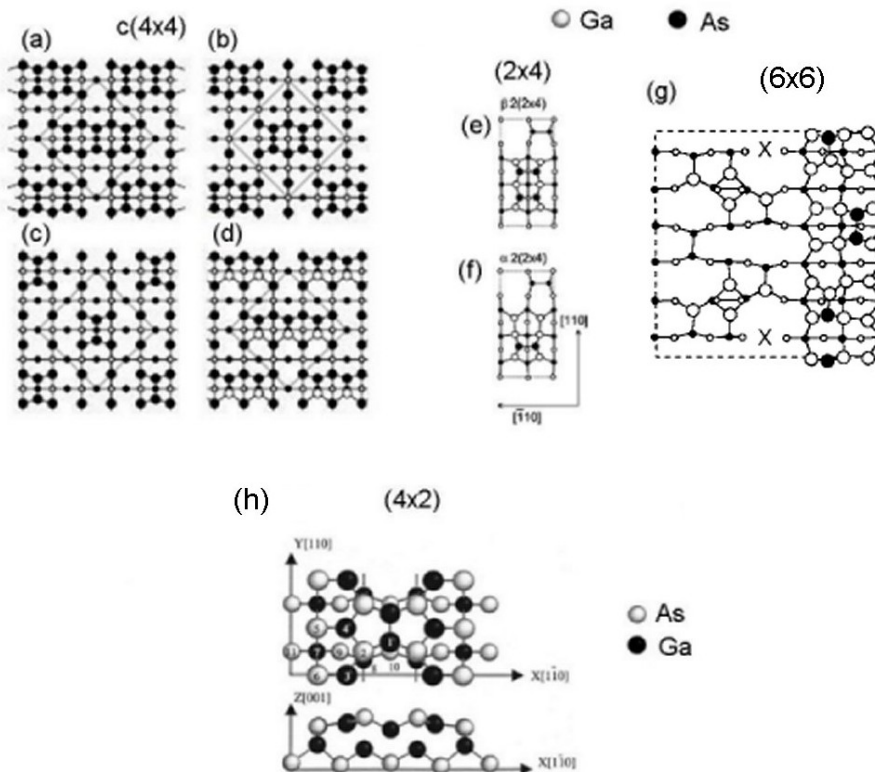

Figure 8. (a-d) Most likely atomic structures for the GaAs(100)c(4x4) surface; taken from ref 25. (e-f) Most likely atomic structures for the GaAs(100)(2x4) surface; taken from ref 26. (g) Most likely atomic structure for the GaAs(100)(6x6) surface; taken from ref 27. (h) Most likely atomic structure for the GaAs(100) (4x2); taken from ref 28.

2.4. Defects

Every real semiconductor crystal contains defects. They are usually categorized into point defects, line defects, planar defects and bulk defects. Point defects include vacancies (missing atoms), interstitial defects (extra atoms between crystal sites), antisites (e.g., As atom in a Ga site in GaAs) and impurity atoms. Dislocations are typical line defects, where atoms of the crystal lattice have misaligned. Stacking fault is an example of planar defect. Bulk defects are regions which often consist of a combination of line and point defects.[9]

The surface of a semiconductor crystal is usually the most defect-rich part of the material. The interaction of the surface with its surroundings is the source of the defects. For example, a semiconductor surface becomes immediately oxidized in air exposure, resulting in an amorphous oxygen-containing surface layer. The thickness of oxidized layer grows in prolonged exposure and saturates around $2 - 5$ nm depending on the material. Oxidized semiconductor surfaces often have much defect states in the band gap. The origin of these states is not understood thoroughly. They are related to vacancies, dangling bonds and different oxide phases. The oxidation of a semiconductor surface is an exothermal process and therefore energetically favored.

Some crystal defects can form even if they are not energetically stable. This can occur, in particular, during the epitaxial growth of thin film stacks. Molecular-beam epitaxy process is affected by kinetics[10] and due to related energy barriers, point defects which are not energetically stable can become buried in the growing crystal. An example of such defect is the As antisite or Ga vacancy formed in the GaAs film which is grown at unusually low substrate temperatures. When growing crystals with chemical vapour deposition (CVD) method, characteristic defects occurring are hydrogen impurities due to hydrogen-containing gases used in the growth. Fortunately, hydrogen atoms can be removed from crystals rather easily by heating, and hydrogen can be useful in the cases where passivation of other defects is needed.

Concerning the synthesis of various junctions of semiconductors, oxidized and

contaminated surface regions can be removed before the deposition of a film, for example, by argon-ion sputtering combined with heating in ultrahigh vacuum conditions. Clean, well-ordered semiconductor surfaces are preferred for growing films and junctions. Still, it is important to note that the semiconductor surfaces have usually a complex structure, reconstruction, as described in a previous chapter, which affects also interface properties. III-V recontructions rarely have atomic ratio of one for group-III to group-V elements; there can be an excess of one element and vacancies as well as dimers in the III-V starting surface on which a junction is constructed. Thus, a reconstruction can lead to the formation of point defects.[10]

It is common to all crystallographic defects that it is not straightforward to experimentally identify them unambiguously. The measurement of local point defects is particularly difficult. The point is that the presence of some defects can be readily concluded, for example, as an impairment of device efficiency or defect related states in band gap, but often the question which defects they are remains open.

Common methods used to characterize semiconductor defects include (i) cross-sectional imaging of crystals by transmission electron microscopy and scanning tunnelling microscopy, which efficiently reveal possible defect clusters and dislocations, (ii) positron annihilation spectroscopy which gives information about the presence of vacancies, (iii) secondary ion mass spectroscopy which provides impurity concentrations for semiconductor crystals.

3. Devices and challenges

III-V semiconductors are currently used in a variety of devices like laser diodes, light-emitting diodes (LED), and transistors. Also high-efficiency III-V multijunction solar cells are intensely developed.

3.1. Examples of devices under development

P-n junction is the heart of many devices (Fig. 9). One side of the junction is doped with substitution atoms (e.g., Si-doped GaAs) that provide extra electrons (n) to the conduction band of the semiconductor and the other side with atoms that provide electron holes (e.g., Be-doped GaAs) (p) to the valence band. A depletion region is formed when the p-n junction is prepared, for example, by growing an epitaxial stack of the n-type and p-type GaAs films. The depletion region forms because part of the extra electrons in the n-type film diffuse towards the p-type film (and vice versa for the extra holes) and recombination occurs. Therefore, the interface region contains ionized dopant atoms, and an electric field is formed. This field compensates the diffusion current, and thus the net current over unbiased p-n junction is zero. The p-n junction can be used with an external electric field or without. For instance, solar cells use the junction without an external field. When an external electric field with forward or reverse bias is applied, the junction can be used as LED or light sensor, respectively.[2,8,9,29]

When the p-n junction is illuminated with light (with energy higher than the band gap), electron-hole pairs are formed. Let's consider the electrons that are excited into the conduction band in the p-side. Those electrons that manage to diffuse to the edge of the depletion region before recombination will move towards the n-side by means of the electric field in the depletion region and contribute to the current produced by light absorption. Vice versa the holes generated in the n-side should reach the depletion-region edge before the recombination to maximize the produced current. Thus, the p-n junction becomes forward biased in a solar cell.[2,9]

P-n junction biased forward is found also in the LEDs, but in LEDs the electron-flow direction is opposite to that in the solar-cell junction. When the external electric field is turned on, electrons in the n-side start to move towards the p-side and eventually recombine with holes producing light. The wavelength of the light depends on the width of the band gap of the material. For light sensors a reverse bias is used. This increases the width of the depletion layer and decreases the diffusion area (diffusion is clearly slower process than the drift). This way the charge carriers can be collected faster at the expense of energy consumption.[2,9]
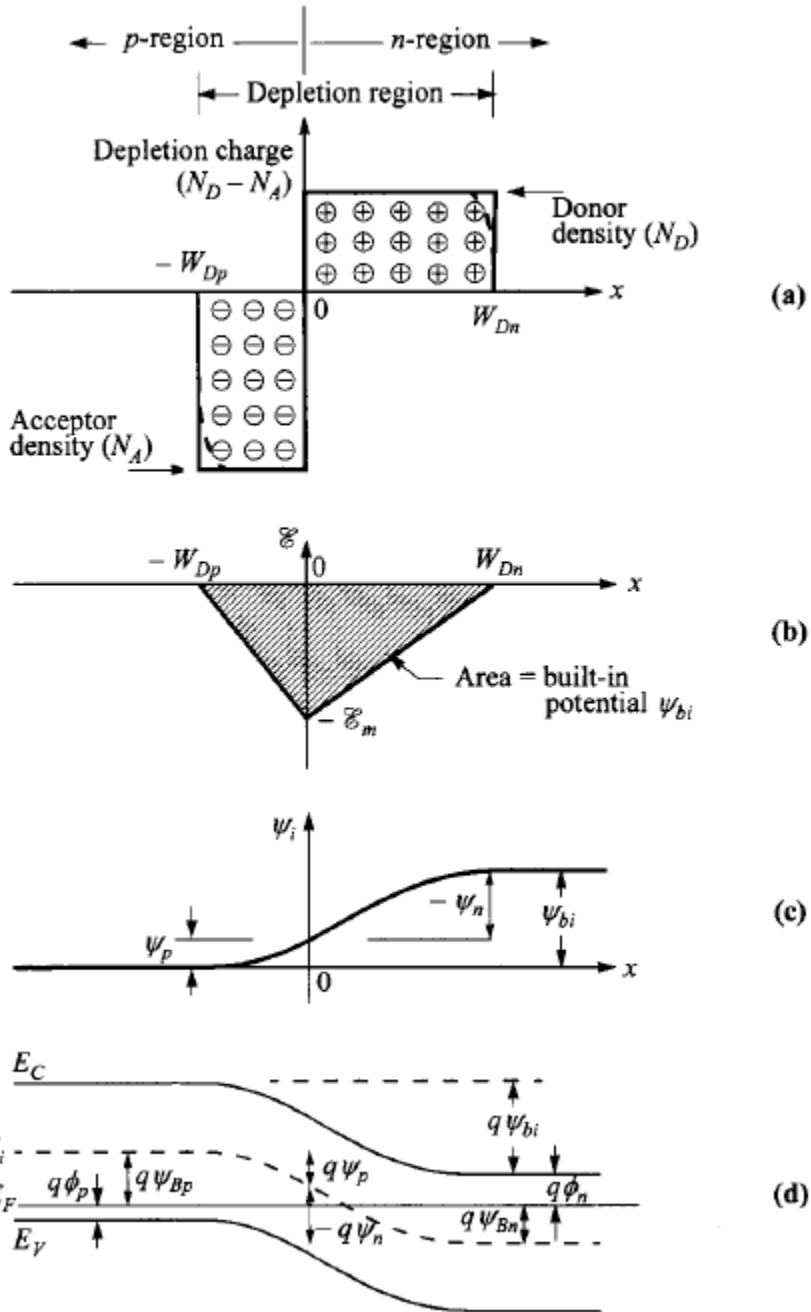
Figure 9. p – n junction in thermal equilibrium. (a) Space-charge distribution. Dashed lines indicate corrections to depletion approximation. (b) Electric-field distribution. (c) Potential distribution where Ψ_{bi} is the built-in potential. (d) Energy band diagram. Figure is taken from ref. 2.

Solar cells transform energy from sunlight to electricity and therefore have many advantages when compared to traditional electricity production by coal and other non-renewable energy sources. Photovoltaic power stations produce no harmful emissions after their manufacture and their upkeep costs are minimal. Nowadays the conservation of nature is a hot topic and utilization of solar energy is an option for safe energy production. World solar cell production and research have increased exponentially in recent years. At the moment, most solar cells are made from silicon but the portion of other materials is on the increase. III-V semiconductors are intensely developed for modern high efficiency multi-junction photovoltaic cells that have layered structure as shown in Fig. 10. These solar cells are expensive, but the concentration of light on a small area of the material provides a potential solution.[30-34]
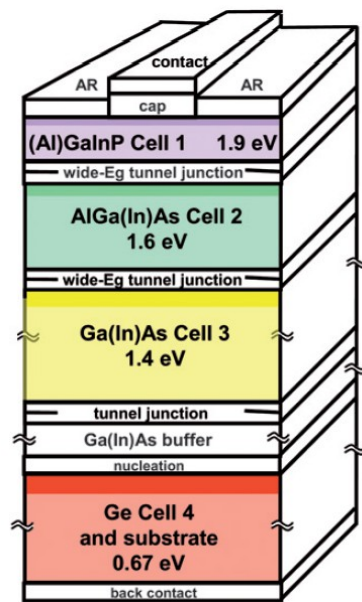
Figure 10. Multi-junction photovoltaic cell made from lattice matched III-V layers. The topmost layer is a protective antireflection coating. Below that there are several semiconducting layers separated by tunnel junctions. Figure is taken from ref. 35.

Commercial photovoltaic cells are mainly made of silicon so far. Their efficiency is 6 % - 20 % depending on the particular design. III-V multi-junction cells (Fig. 10) have been developed intensively because they have higher efficiency than the Si

cells. Their efficiency is around 30 %, and can be improved to about 45% when using concentrated sunlight. It is worth noting that if the incoming photon has less energy than the band gap of the semiconductor it cannot create an electron-hole pair and therefore cannot be absorbed. On the other hand, if the photon has much greater energy than what is needed to excite an electron from the valence band to the conducting band some of the energy is lost to collisions and transformed into heat. A design such as described in Fig. 10. can overcome these problems. The most energetic photons are absorbed in the topmost layer which has the highest band-gap. Photons with less energy will pass through to the next layers and are absorbed eventually as the band gap gets smaller.[30-34]

Lighting with LEDs is another growing III-V market with annual growth rate of about 30 %. LED bulbs have an important advantage compared to traditional light bulbs and compact fluorescent lamps. They consume only a fraction of the power and have the same or better luminescence. LED bulbs are more expensive but lower operating costs combined with longer lifetime bring savings. Other major appliances for III-V LEDs are TVs and displays. LED colors range from infrared to ultraviolet.[36]

The invention of transistor was an important step in the history of electronics.[37] Modern way of life would not be possible without it. Transistors can be found in every kind of electronic applications. Integrated circuits used in computers can have billions of transistors packed in an area the size of a matchbox. III-V materials are already used in transistors, most notably high electron mobility transistors (HEMT) in cellphones. Development is underway to make III-V channel metal-oxide-semiconductor field-effect transistors (MOSFET).[1,3] MOSFET schematic is shown in Fig. 11.
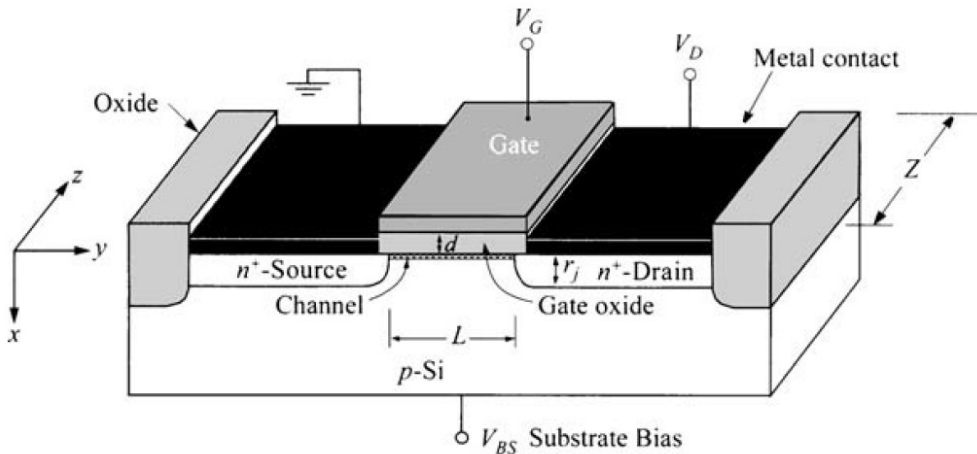
Figure 11. MOSFET schematic. Figure is taken from ref 2.

Transistor is a device which can control the flow of current from source to drain by using gate voltage. A conducting channel is formed at the gate oxide-semiconductor interface when a sufficiently large electric field, known as the threshold voltage, is applied between gate and body. Since the current flows in the vicinity of the interface it is strongly affected by defects at the interface. The inherent inferiority of III-V semiconductor interfaces with insulators, when compared to silicon, has been a major focusing point of III-V transistor development.[1,2,12,21]

Most transistors in the world are made of silicon. Compared to silicon, III-V materials have advantages but they also have drawbacks. Many III-V semiconductors have much higher charge carrier mobilities than silicon. As already remarked, the higher mobility allows the device to operate at higher frequency. One significant drawback is that III-V semiconductor interface with insulating layer has a high defect density, much higher than in the commercial Si-based MOSFET, which has hindered the use of III-V's in MOSFETS. After a passivation (e.g., with hydrogen) of the oxide-silicon interface, its defect density around the band gap is $1\text{-}10\times10^{10}$ states/cm^2/eV. For III-V's the interface defect density has been around 10^{12} or higher but recently for III-V/oxide interface a value of about 10^{11} has been achieved.[2,3,21]

A well known concept in electronics is the Moore's Law. Gordon Moore published

in 1965 an article where he predicted that the number of components in an integrated circuit will double every two years.[38] This behavior is now known as Moore's Law. His prediction has been correct so far but it is unclear how far into the future Moore's law will hold. The reason for this is a miniaturization of the components. The smallest details of an IC are already well in the nanometer scale and further reduction in size becomes more difficult. The minimal size of the components creates problems such as leakage current. Also, the manufacturing process must be controlled extremely well because even the slightest variations might render the component unusable.[4] Problems like these have driven the research of alternative materials such as III-V semiconductors, which theoretically offer better electrical properties when compared to silicon.

Quantum mechanical phenomena become visible when the dimensions of a transistor are sufficiently small. Tunneling current through the gate oxide, also known as leakage, is an example of this. Nowadays the component is so small that the oxide film is only a few atomic layer thick and the leakage can readily occur. One solution is to replace the silicon dioxide with some other material with a higher dielectric constant, such as Hafnium dioxide, which allows the reduction of the leakage current. Such materials are usually referred to as high-κ dielectrics.[2,39] The leakage current becomes larger and larger as the dimensions get smaller. As of 2014, the smallest gate lengths used are less than 20 nm.[1] In order to improve devices even further it is necessary to find new materials to replace silicon as the channel material and III-V's are potential candidates for this.

3.2. Challenges in the preparation and characterization of device materials

As mentioned above, the preparation of oxide/III-V interface for MOSFET is one of the biggest challenges in the semiconductor science and technology at the moment. That interface has been researched and developed for more than 40 years. It is now clear that the oxide/Si interface is unique among the interfaces. Both the natural structure of SiO_2/Si interface and the possibility to passivate its defects makes it superior. It is also clear that uncontrolled oxidation of III-V surfaces during the manufacturing of any insulator film on the III-V surface causes a high

density of interface defects.[3,40,41] However the atomic-scale understanding of these defects is far from complete. This is understandable because it is difficult to characterize local defects below the surface with atomic resolution. A big problem that is difficult or even impossible to avoid is the oxidation of III-V surfaces during the interface growth. Also, the rise of devices utilizing nanotechnology has emphasized the need to understand and control properties of surfaces and interfaces.

Common methods to characterize averaged material compositions including defect concentrations are secondary ion mass spectroscopy,[42] and Rutherford backscattering spectroscopy.[43,44] These have been successfully applied to probe the bulk defects, but it is unclear how powerful they are to characterize quasi-two-dimensional interfaces.

Scanning tunneling microscopy[45] (STM) has been utilized to study local defects on surfaces, but the relevant defects are located at the buried interface. STM can be also employed to study defects observed on cross-sectional surfaces across the interface. However it is sometimes unclear what kind of effects the cleaving has on the observed defects. Furthermore, the identification of features observed in STM images is not straightforward in general. Transmission electron microscopy (TEM) is another local probe which has been utilized in atomic scale resolution imaging of oxide/semiconductor interfaces.

Concerning solar-cell development, one key material system is the dilute nitrides GaInAsN. These films can be integrated into GaAs-based multijunction stacks to absorb the infrared part of the solar spectrum so that high crystal quality of the stack remains (i.e., the lattice matched system). The problem is that the incorporation of N atoms into the crystal (some As atoms are replaced with N atoms) causes unusually high defect concentrations.[46,47] Furthermore, it is again challenging to study local N-induced defects with atomic resolution, and the origin of these defects has remained a mystery.

InN has also proven a challenging material because InN films usually contain high unintentional electron concentrations, in particular at the polar InN(0001) and InN(000-1) surfaces. Reports indicate that the origin of these extra electrons is

related to the surface quality of InN, and so far the surface Fermi level of polar InN has been argued to lie in the conduction band.[48,49] Thus, a key question is how we can modify the InN surface so that the Fermi level position can be tailored.

3.3. Goals of the work

The main goals of this work are: (1) to improve the understanding of the structures of both harmful and non-harmful oxidation-induced defects at insulator/III-V interfaces as well as the structures of N-induced defects in GaInAsN materials, (2) to develop the method for modifying properties of insulator/III-V interfaces, and (3) to find a method to decrease the unintentional electron concentrations of InN films.

4. Experimental methods

Most of this thesis research was done using an X-ray photoelectron spectroscope (XPS) and therefore the concept of this technique is described in chapter 4.1. Chapter 4.2 decribes the use of an alternative photon source in the form of synchrotron radiation (SRPES). Low-energy electron diffraction (LEED) is described in chapter 4.3, photoluminescence (PL) in 4.4 and scanning tunnelling microscopy/spectrsoscopy (STM/STS) in 4.5. With the exception of paper 5 all the results presented in this thesis come from experimental research. Paper 5 contains also calculational results which were obtained using Vienna *ab-initio* simulation package (VASP). The details of VASP and related calculational concepts will not be reviewed here. The reader can find more information about calculations in references 50 – 53.

4.1. X-ray photoelectron spectroscopy

X- ray photoelectron spectroscopy (XPS) is based on the photoelectric effect which was discovered by Heinrich Hertz in 1887[16] and described mathematically by Albert Einstein in 1905[54]. The Nobel Committee recognized Einstein's findings and Einstein received a Nobel Prize in physics in 1921 for his discovery of the law of the photoelectric effect.[55] XPS is a technique with which the elemental composition and the chemical bonding environments in the sample can be probed, as its other name ESCA (Electron Spectroscopy for Chemical Analysis) suggests. Also, XPS is a non-destructive method and can be used in conjunction with other techniques to gain maximal understanding about the task in hand. It is a rather surface sensitive method where the sample surface is irradiated with x-rays. This causes electrons to be emitted from a sample due to photoelectric effect. These electrons are called photoelectrons and are collected at the detector.[56,57]

The kinetic energy of a photoelectron (E_k) depends on the energy of the photon ($h\nu$) and the binding energy of the electron (E_b). Also, when the electron is collected at the detector, the work function of the detector (Φ) has to be taken into account.

$$E_k = h\nu - E_b - \Phi \qquad (1)$$

Photoelectron spectroscopy can be a useful tool when studying the properties of semiconductor devices and can be used to probe various interfaces if they are not buried too deep beneath the surface. As interfaces are of utmost importance to device performance it is important to have thorough knowledge of them. Nobel laureate Herbert Kromer has even said: "The interface is the device."[58] By using state-of-the-art synchrotron radiation sources, the probing depth of buried interfaces can be further increased.

The most common x-ray tube anode materials in traditional XPS are Al and Mg. The K_α photons for those elements have energies of 1486.7 eV and 1253 eV, respectively, and the energy broadening is about ~1 eV. However, XPS instrument can be equipped with a monochromator narrowing the energy dispersion of photons

and therefore improving the resolution to less than 0.5 eV.[60]

A typical XPS survey spectrum is shown in Fig. 12. Each element has characteristic electron binding energies with which the elements can be identified. The material composition can be estimated from the peak intensities taking into account the different photoelectron excitation probabilities for different core levels. In other words, not all elements are equally sensitive to XPS. There is great variation in the sensitivity factor and it ranges from 0.025 for lithium to over 10 for heavy elements. For example, when studying LiF, the peak areas of Li 1s and F 1s would be very different even though the material contains the same amount of atoms from each element, because F 1s sensitivity (1.000) is 40 times greater than Li 1s (0.025). The trend is that heavier elements are more sensitive, because they scatter photons more efficiently and therefore have higher photoionization cross-section. Although H and He can in principle be studied with XPS, in contrast to Auger electron spectroscopy, which is the other traditional method for elemental analysis, in practice their sensitivity is too low.[56]
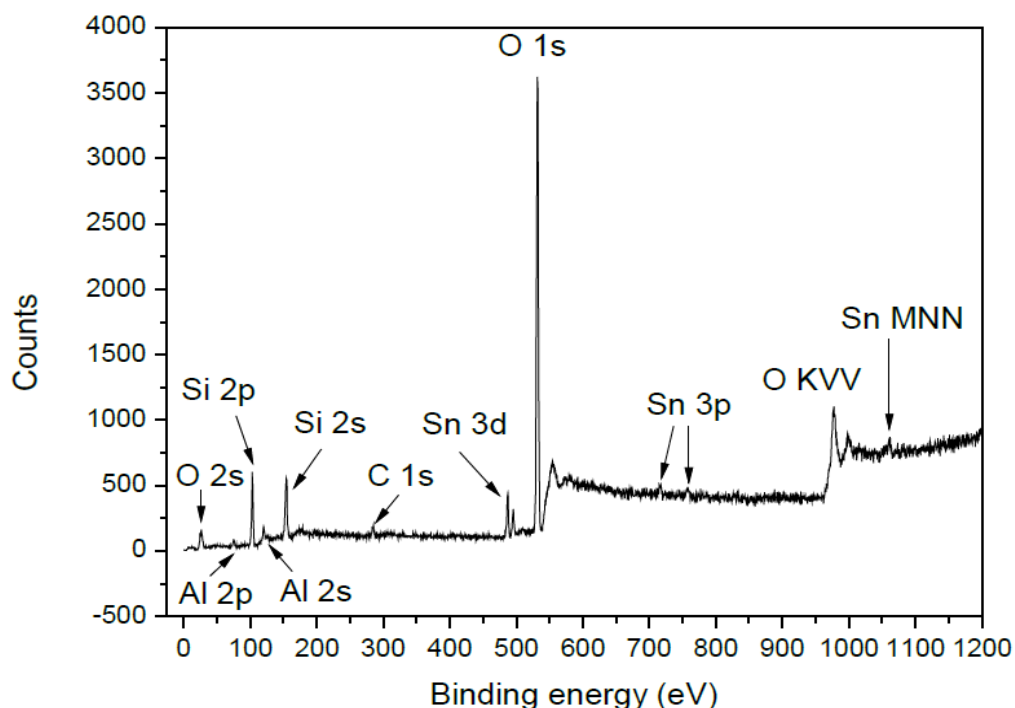

Figure 12. XPS survey spectrum from Sn and Al containing SiO_2 powder sample.

It is beneficial to take also high-resolution spectra with a small energy step to obtain more precise results. A high-resolution spectrum can be seen in Fig 13.
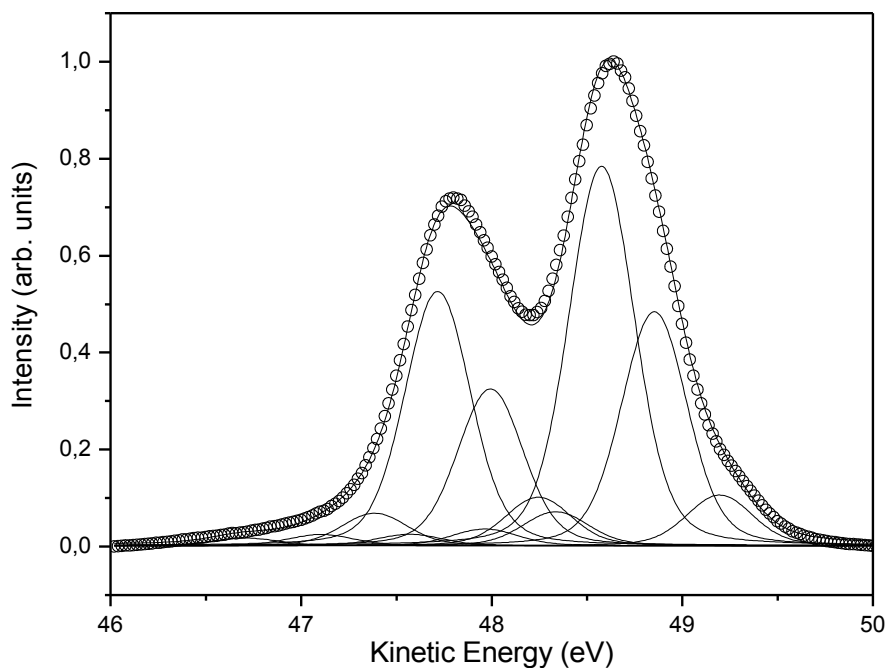

Figure 13. A high-resolution XPS spectrum.

In addition to the elemental analysis, the chemical environments of elements can be studied on the basis of high-resolution photoelectron spectra. If there are more than one chemical environment they manifest themselves as distinct peaks or as shoulders in the peak depending on the difference in binding energy. A difference in chemical environment means here that the initial electronic potential or/and the response of other valence electrons to the creation of core hole in the final state (so-called screening and relaxation effects) is/are different for the non-equivalent atomic sites.[61]

Some of the considered differences can arise from the surface reconstruction. This is because the electronic environment of the surface atoms is different from bulk atoms. Such differences in core-level binding energy are called surface core level

shifts (SCLS). They are usually resolved using synchrotron radiation photon source because traditional XPS might not have good enough resolution and with synchrotron radiation the photon energy can be tuned to get more surface sensitive signal.

The universal curve is useful to estimate the escape depth of photoelectrons analyzed in XPS. It shows the inelastic mean free path of electrons travelling in a solid. The probing depth is around three times the mean free path. Basically the universal curve is not dependent of the material used even though there is some variation.[62] The universal curve is especially useful when using synchrotron radiation and choosing appropriate photons energies because this allows the user to optimize the probing depth and identify surface and bulk related contributions in a measured signal. The universal curve is shown in Fig 14.
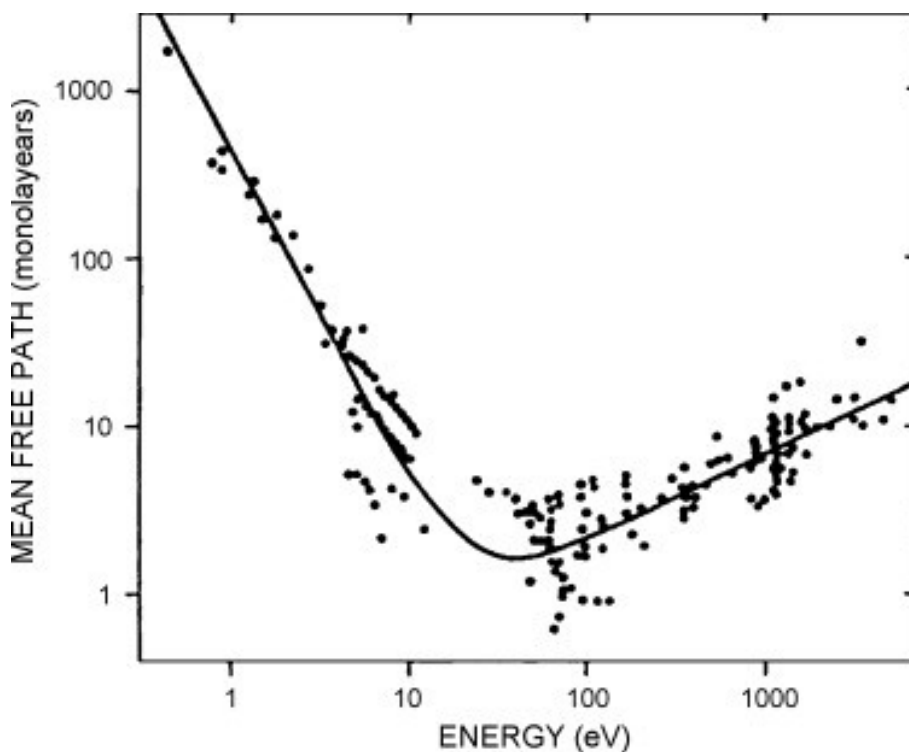

Fig 14. The universal curve. Figure is taken from Ref. 62

4.2. Synchrotron radiation photoelectron spectroscopy

The operation principle of a synchrotron was first published by Vladimir Veksler in 1944[63] and the first working synchrotron was constructed by Edwin McMillan in 1945[64]. Nowadays synchrotron radiation facilities are quite large investments. For example, just the phase I of MAX IV has an estimated cost of over 100 million euros.[65] Nevertheless, there are tens of synchrotron facilities around the world. They offer clear benefits in many different research areas. Synchrotrons have been traditionally used by physicists and recently chemistry and life science synchrotron research has gained popularity.

Synchrotron radiation photoelectron spectroscopy (SRPES) has several advantages when compared to traditional XPS. In addition to the tuned photon energy, the luminosity is much brighter at the synchrotrons. The photon source broadening is smaller (i.e., better energy resolution) than in ordinary XPS. Electrons are first injected into the storage ring by a linear accelerator (LINAC). In the storage ring they are kept in a circular course with bending magnets. Bending magnets, wigglers and undulators are used to create photons which are utilized in experimental stations. The electrons lose energy as they emit radiation and an RF cavity is used to maintain the electrons in the storage ring.[66]

It was discovered in 1897 by J. J. Larmor that accelerating charged particles emit light.[67] The Larmor formula gives the total power radiated by a particle

$$P = \frac{q^2 a^2}{6\pi\varepsilon_0 c^3} \tag{2}$$

where q is charge, a is acceleration, ε_0 is vacuum permittivity and c is speed of light. The angular distribution can be shown to be

$$P = \frac{q^2 a^2}{4\pi c^3} \frac{\sin^2\theta}{(1 - \beta\cos\theta)^5} \tag{3}$$

where θ is the angle between velocity and observer, $\beta = \frac{v}{c}$ and v is the velocity of the particle.

In addition to bending magnets, synchrotrons are usually fitted with wigglers and undulators which work in a similar way to create light. They both have magnets with opposing polarity side by side causing the electrons to wiggle, hence the name. Undulators and wigglers use different magnetic field intensity and different spacing of magnets to create photons. Wigglers have a broad energy spectrum and undulators small. This difference is because radiation created in the undulator undergoes interference whereas radiation from the wiggler does not.[66] Fig. 15. shows an undulator schematic.
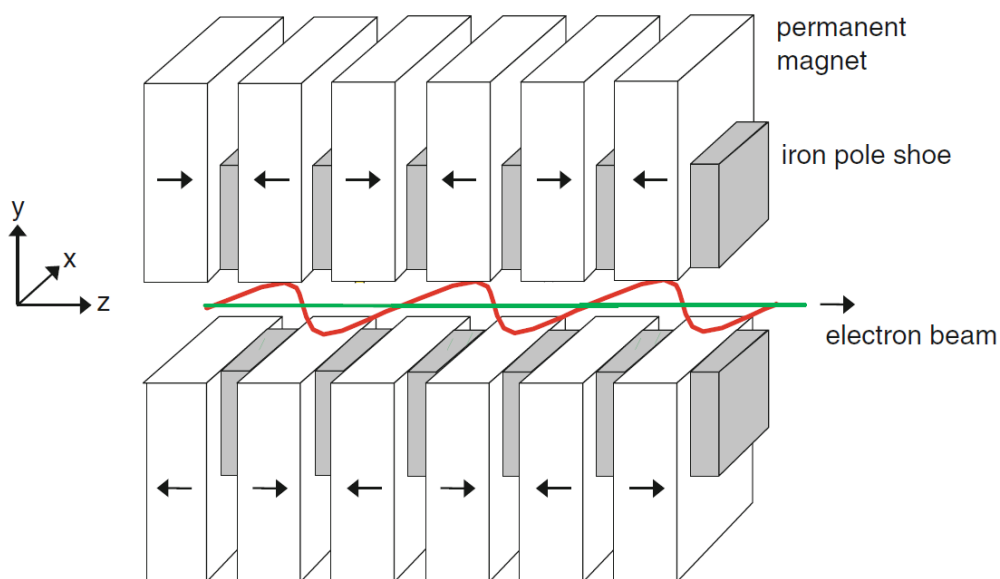

Fig. 15. Schematic view of a planar undulator magnet with alternating polarity of the magnetic field and of the sine-like trajectory of the electrons. Figure is taken from ref 68.

Part of this thesis research was conducted at MAX-lab synchrotron facility located at Lund University, Sweden. The beamlines used were I4, which is connected to the MAX-III ring, and I311, which is connected to MAX-II ring. The photon source of both is an undulator. The photon energy range is 14 eV – 200 eV at I4 and 43 eV – 1500 eV at I311. The analyzers are two dimensional detector SPECS Phoibos 100 and hemispherical electron energy analyzer SCIENTA SES200, respectively. Both have energy resolution E/dE about $1 \cdot 10^4$.[69,70]

The tunable photon energy is especially useful property of a synchrotron since the photoionization cross-section depends on the photon energy. Traditional XPS uses over 1 keV photons and these have very low cross-section with valence band electrons. With a synchrotron, it is possible to use photons with significantly lower energies and therefore get much higher signal-to-noise ratio. The change in cross-section can be several orders of magnitude. It can be also useful to control the surface sensitivity of the measurement by tuning the photon energy. As mentioned previously, the inelastic mean free path of an electron in a solid depends on its kinetic energy.[66]

It is also possible to vary the angle of photoemission. Photoelectrons collected at a normal angle to the surface provide information about deeper layers of a sample as compared to the electrons collected at a grazing angle. This difference makes it possible to enhance the surface sensitivity when setting the emission angle away from the sample surface normal. When comparing spectra taken at different emission angles, it is possible to identify the spectral features which are related to atoms at a surface and the features which are related to atoms in the subsurface region or/and in the bulk. Theoretical calculations can also be useful in identifying the atomic origins of spectral features.

One weakness of PES is the difficulty to conclude unambiguously origins of spectral changes. Literature references are important and also it is helpful to combine calculated SCLS based on different atomic structures to gain a better understanding. Furthermore, several different components might overlap in the spectrum measured. In the analysis it is necessary to deconvolute the spectrum into separate components by using a computer program. In order to get a well-justified fitting, several physically reasonable constraints need to be included in the fitting program. Because the PES signal arises from a macroscopic surface area, it is also essential to have well-defined samples clean from contaminations to gain the best understanding.

4.3. Low energy electron diffraction

With low energy electron diffraction (LEED) the surface structure periodicity can be studied easily. In this technique an electron gun is used to produce a monochromatic primary beam of low energy electrons travelling towards the sample. The electrons are elastically back scattered by the surface layers and their angular distribution observed at a fluorescent screen provides the information about the surface structure. Background of inelastic electrons is removed by a retarding field.[71] Low energy electron diffraction was discovered in 1927 by C. Davisson and L. Germer[72], but it took decades for it to become a widely used technique. This is partly because at the time of its discovery the vacuum technology was still very immature. The electrons from an electron gun must not inelastically scatter with gas molecules until reaching the fluorescent mesh where the diffraction pattern is seen. This limits the pressure inside the analyzing chamber to ultra-high-vacuum. The sample surface must also be well-ordered and crystalline. No diffraction pattern is observed from an amorphous surface layer.

When the electron beam hits the sample surface it can elastically scatter. The beam of elastically scattered electrons can be represented by a plane-wave with a de Broglie wavelength of

$$\lambda = \frac{h}{\sqrt{2mE}} \tag{4}$$

where h is the Planck constant, m is the electron mass and E is the electron kinetic energy. The pattern formed at the LEED screen is a visualization of the reciprocal lattice of the sample surface. An example of this is shown in Fig 16. Constructive interference strengthens those waves in a same phase.[71]
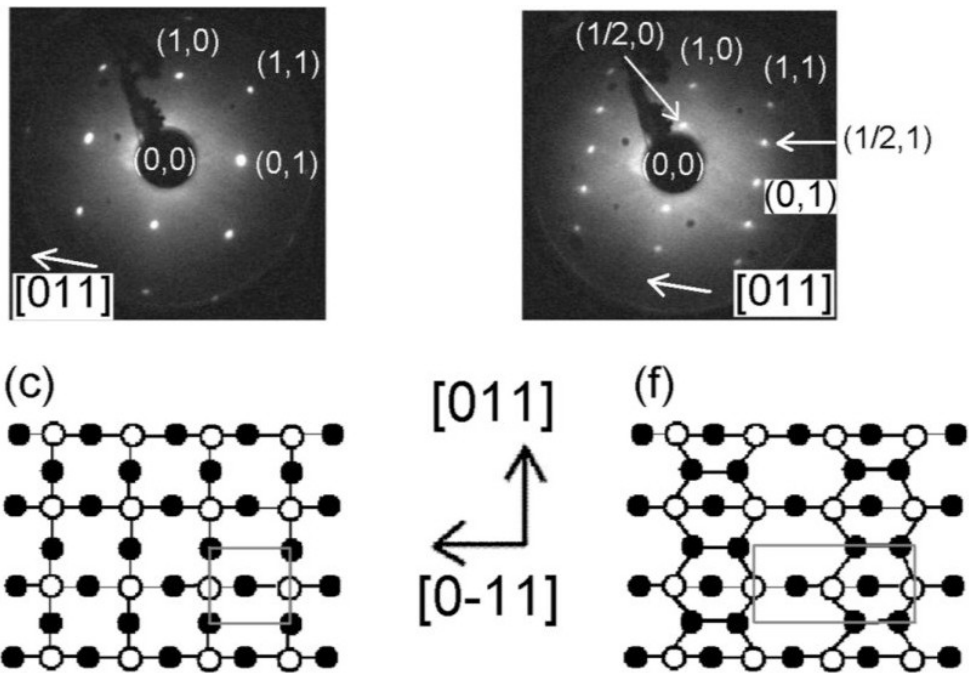
Figure 16. Low-energy-electron-diffraction (LEED) example patterns visualizing the reciprocal lattices in the real space. Figure is adapted from ref 71.

To obtain a LEED pattern one must first prepare a clean crystalline surface. This can be done in a vacuum by cleaving the sample, by using a chemical or a heat treatment, or by argon sputtering. The sample must be set perpendicular to the electron beam. Typical electron kinetic energies are from 20 eV up to 200 eV. According to the universal curve, in this energy range the surface sensitivity is highly enhanced. The reflected electrons are collected at a hemispherical screen. Inelastically scattered electrons are deflected by a grid with an applied retarding field before reaching the screen. The diffraction pattern is usually recorded with a digital camera for further analysis. Figure 17 shows the experimental setup for LEED.
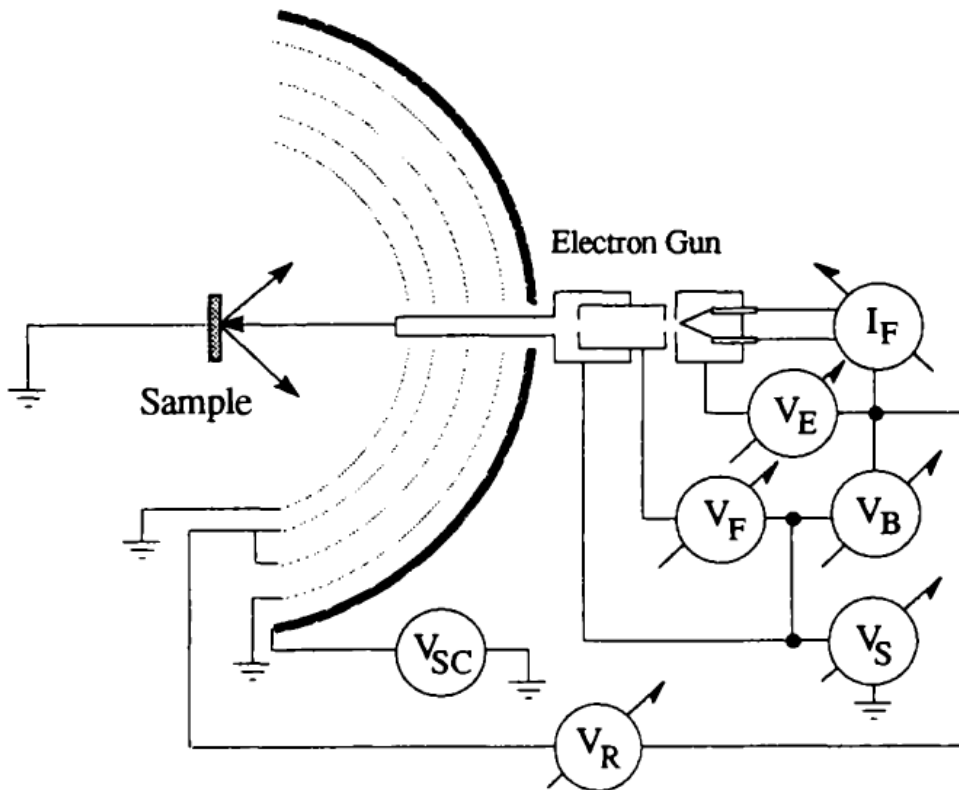
Fig 17. LEED Schematic. Figure is taken from ref 73.

The intensity of individual spots in the diffraction pattern can vary significantly. This depends on the electron energy as well as the specific type of surface reconstruction.

LEED provides quickly important information about the crystal quality and lattice type of sample surface parts. However, LEED is not sensitive to local surface defects. There are examples of surfaces which produce a reasonable LEED pattern but the surface still include a high density of surface defects observer in microscopy images. That is, surprisingly small areas with crystalline structure provides a sharp diffarction pattern.

4.4. Photoluminescence

Photoluminescence (PL) is a technique which is in widespread use in semiconductor research and technology. It is especially used in the development of optoelectronic devices. This is because of several reasons. PL is one of the few techniques to probe the all-important interfaces without destroying the sample. PL measurements are usually straightforward and require very little or no sample preparation and therefore they can be done fast. Also, PL measurements can be done at room temperature and air pressure.

Depending on what is the objective of the study, the focus of the PL spectral changes can be on intensity, wavelength, time dependence, spatial dependence or temperature dependence. These different parameters give different kinds of information about the sample. Information about the purity and crystalline quality of the sample can be obtained with PL intensity measurements. Time-resolved luminescence gives us information about the minority carrier lifetimes and recombination mechanisms. Spatial measurements can tell about interface uniformity and temperature dependence measurements about the depth of long-lived traps.[59,71]

Although PL is commonly considered as a bulk probe, PL intensity is very sensitive to the quality (defect density) of a surface part of the semiconductor. Excited charge carriers, particularly electrons in conduction-band, have a long diffusion length (100 nm) and can easily reach the sample surface and undergo recombination there using defect states in the band gap.

When sufficiently energetic photons hit a semiconductor sample, they excite electrons to the conduction band due to photovoltaic effect. When the electrons return to their ground state, radiative relaxation can occur. This is called photoluminescence. Semiconductors with a direct bandgap are much better suited for PL measurements than semiconductors with an indirect bandgap. This is because in an indirect bandgap the radiative recombination of an electron-hole pair requires the absorption or emission of a phonon.[59]

The choice of photon source for excitation is important and laser light is the natural choice. Laser offers many benefits such as being monochromatic and collimated. The experimental setup for PL measurements is simple and shown in Fig. 18. A sample is illuminated and photons from radiative relaxation are collected with a lens to a spectrometer or a photodetector. The penetration depth of excitation photons is dependent on their energy. The energy also defines the initial excited state. For direct bandgap semiconductors illuminated with photons with energy greater than the bandgap width, the penetration depth is of the order of 1 μm. The penetration depth is much greater when using photons with energy less than the bandgap or when studying indirect bandgap semiconductors.[59]
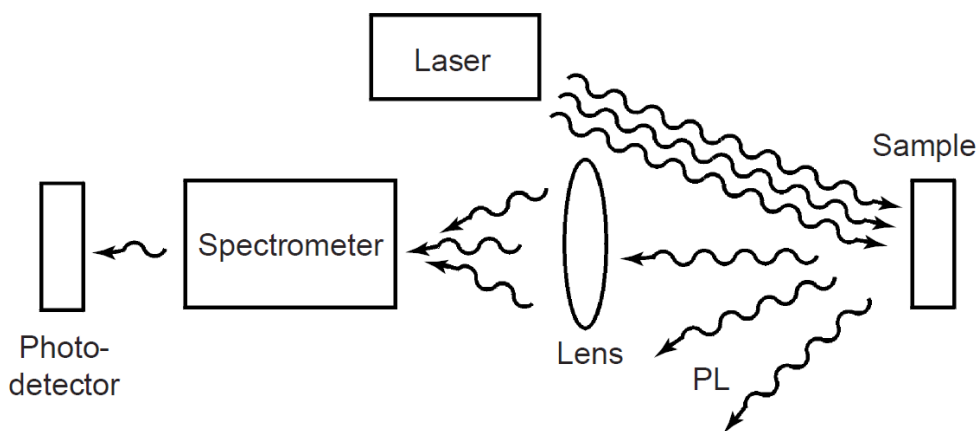

Fig 18. PL schematic. Figure is taken from Ref. 59.

If there are defect states in the band gap, some of the photons from radiative recombination will have smaller energy than the band gap. Excited electrons can also go through nonradiative recombination if there are defect states in the midgap position. When there are lots of defects there are also lots of nonradiative relaxation. Large PL signal correlates with good interface properties, i.e. low defect density. Also, when studying interface defects the laser intensity is important. Since there is a finite number of interface states the PL signal will saturate when using large power laser.[59,71]

The PL spectral changes at the interface are easy to evaluate qualitatively. If the PL signal increases, e.g. after rapid thermal annealing (RTA), the nonradiative recombination at the interface has decreased. This reduction of nonradiative

recombination is called surface passivation and is the goal of many surface treatments.[59]

Because electrons and holes have different masses, donors and acceptors have different binding energies. Dopant levels which are either near the VBM or CBM are called shallow levels and they are more likely to participate in radiative recombination provided that the sample temperature is small enough so that the carriers are not thermally activated out of the traps. Deep levels reside in the midgap and facilitate nonradiative recombination by providing a stop-over for electrons making their way between the conduction and valence bands by emitting phonons. Dangling bonds often provide numerous midgap states that facilitate rapid nonradiative recombination.[59]

Information about the interface alloying can be gained by studying the PL signal peak position. The bandgap of a semiconductor is dependent on alloy composition, and in the PL measurement, excited electrons and holes transfer quickly to the conduction- and valence-band edges, respectively, before recombination. Interface roughness tends to produce line broadening and surface recombination velocity is proportional to the density of surface states.[59,71]

PL provides quickly qualitative information about crystal quality and defect density, but determination of absolute defect density is not straightforward. Radiative emission through the defect states in the band gap gives information about the position of the defect levels in relation to the band edges. However, the identification of the origins of such gap states is challenging.

4.5. Scanning tunnelling microscopy/spectroscopy

Scanning tunnelling microscopy (STM) is a rather new tool surface scientists use. It was developed in 1981 by Gerd Binnig and Heinrich Rohrer.[45] They were awarded the Nobel prize in physics in 1986 for their invention.[74] STM is one of few imaging techniques capable of atomic resolution. In addition to obtaining a topographical image of a surface, it can be used in a spectroscopic mode giving

information about the local electronic structure of a surface.

STM utilises the quantum mechanical tunnelling effect. An atomically sharp tip, preferably one atom thick at the apex, is brought close (< 1 nm) to the sample surface. Then an electric potential difference is set between the tip and the sample. This causes electrons to flow from the tip to the sample, or vice versa, depending on the sign of the applied bias. STM schematic is shown in figure 19. The tunneling current is inversely proportional to the distance of the tip and the sample, [75]

$$I = Ue^{-2\frac{\sqrt{2m\Phi}}{\hbar}D}, \qquad (5)$$

where U is the voltage between the sample and the tip, m is the electron mass, Φ is the work function of the sample, $\hbar$ is the reduced Planck constant and D is the distance from the tip to the sample. Since the dependency is exponential the tunnelling current rapidly diminishes with increasing distance.
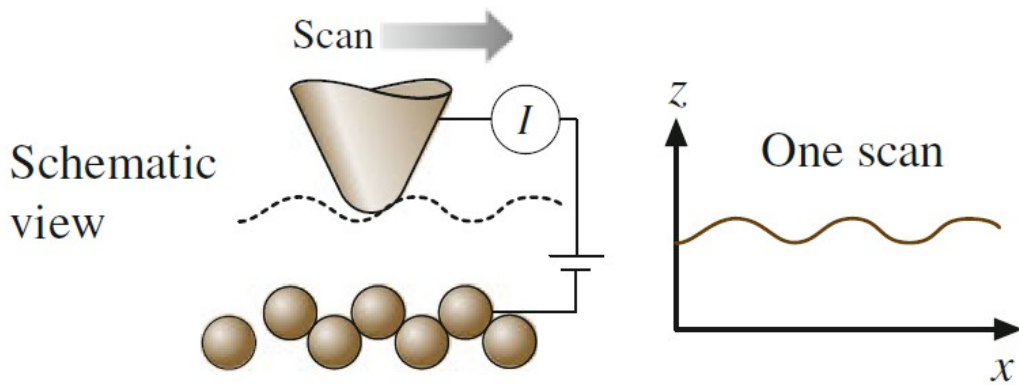

Fig 19. STM schematic. Figure is adapted from ref. 76.

The tip is firmly attached to a piezoelectric crystal. Piezoelectric materials generate a voltage when their shape or size is changed. This works also the other way around: When applying a voltage to a piezoelectric crystal, it undergoes deformation. This way it is possible to use STM in either constant height mode or constant current mode. In constant height mode the vertical position of the tip is constant over the surface and the tunnelling current I(x,y) is measured. This way

34

pits on the surface give smaller current than bumps do. In constant current mode the tunnelling current is kept constant over the surface and the vertical position of the tip z(x,y) is measured.[75]

STM imaging can be done in a filled state mode where electrons flow from the sample to the tip giving information about filled electronic states, or empty state mode where electrons flow from the tip to the sample giving the distribution of empty states. These two modes require applying opposite biases. It is essential that the obtained images do not represent the actual positions of atoms but a spatial distribution of density-of-states of electrons.[75]

Scanning tunnelling spectroscopy (STS) is a complementary technique for measuring the electron density at a surface. In STS the tip can be stopped at a selected position and the current-voltage (I-V) curve is measured. I-V curves can also be measured over a selected surface area at different points, making a map of distribution of electronic states. By measuring the I-V curve it is possible to obtain density-of-states (DOS) images, where valence band, conduction band and the band gap between them can be seen. This is done by normalizing and differentiating the initial curve.[77]

STM and STS are an irreplaceable tool in nanoscience development. They provide a unique opportunity to investigate various phenomena on solid surfaces with atomic resolution in real space. Usually a very smooth surface area is prepared for atomic-scale imaging. Large-scale STM images are also useful to make conclusions about the quality and defect density of semiconductor surfaces, for example, after a cleaning procedure and before starting a junction synthesis. Ab initio calculation based simulations of STM images are often used to help identify features seen in experimental STM images. Without simulations identification is challenging.

5. Results

The common topic and the main responsibility of the author for all the articles included in this thesis is the use of photoelectron spectroscopy. XPS or SRPES studies were done in combination with complentary methods to obtain the chemical bonding environment of insulator/GaAs(100) interface in paper 1, to study the growth and properties of crystalline BaO on the GaAs(100) surface in paper 2, to study the formation of InN and its valence band in paper 3, to study the fabrication and surface passivation of GaAs nanoparticles in paper 4, and to study Ga interstitials in GaAsN in paper 5. These results will be briefly summarized in this chapter.

5.1. Insulator/GaAs interface study (paper 1)

As discussed in previous chapters the interface quality of insulator/semiconductor junctions is very important. In this paper the chemical composition of SiO_2/GaAs and SiN_x/GaAs interfaces of GaInAsN/GaAs quantum-well heterostructure samples is studied using XPS and PL. A set of three samples for both insulators was prepared: as-grown, 80 s rapid thermal annealing (RTA) and 1000 s RTA. During device manufacturing process it is common that the wafers are annealed in elevated temperatures for short periods of time. It is known as RTA.

XPS measurements revealed Ga_2O (i.e., GaO_x in Fig. 20) formation at the insulator/semiconductor interface after RTA and simultaneous PL intensity increase for both SiO_2/GaAs and SiN_x/GaAs. As mentioned in a previous chapter, PL intensity is inversely proportional to defect density at the interface and therefore Ga_2O can be linked to being useful at the interface. Figure 20 shows Ga 3d spectra and the related PL spectra.
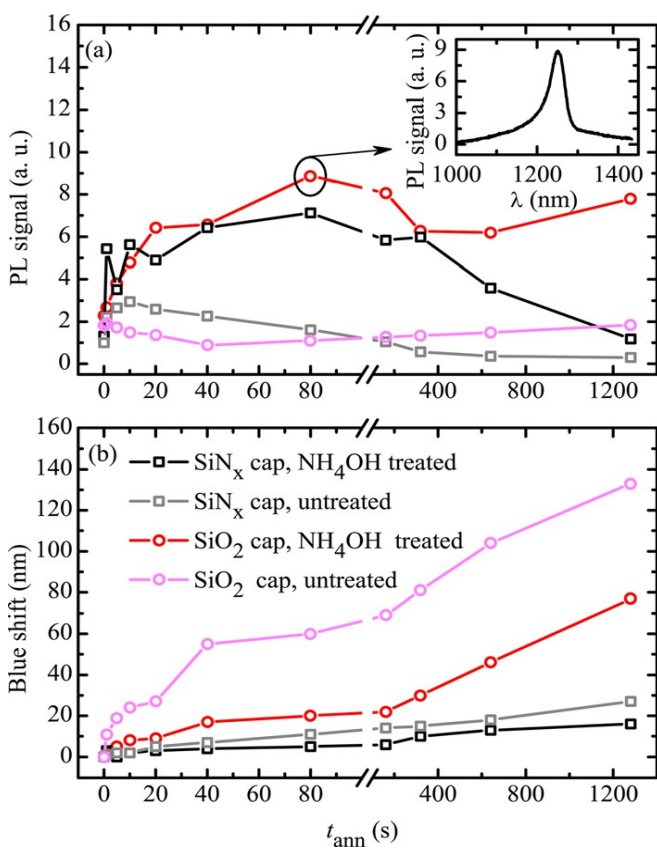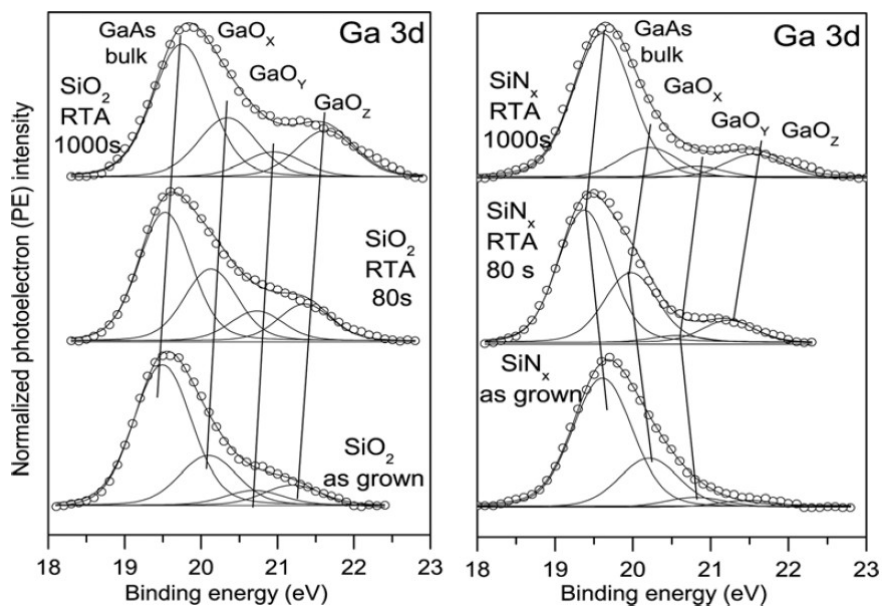
Figure 20. Ga 3d spectra and corresponding PL results.

The XPS spectra from As 3d revealed an additional component besides the one from Ga-As bulk, shown if Fig. 21. This is attributed to As-As defect bonding as previous calculational studies suggest.
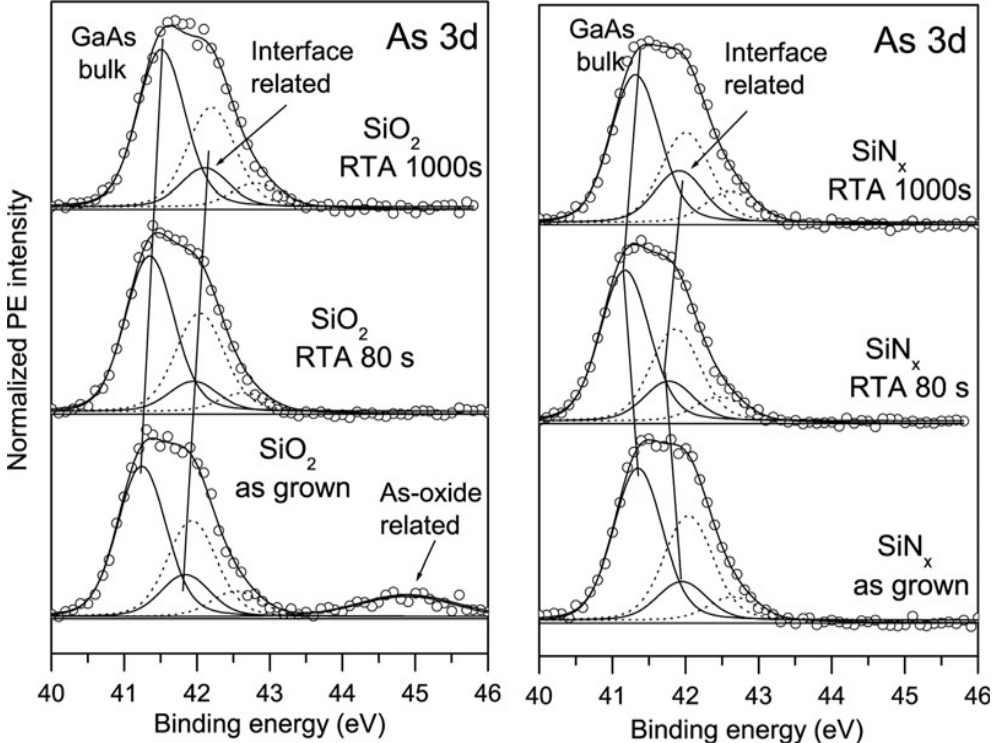

Figure 21. As 3d spectra showing both the bulk Ga-As component and the As-As component.

Also the diffusion of Ga atoms (GaO_z component in Fig. 20) but not As atoms into the insulator was observed. Evidence for this can be found in the Ga 2p and As 2p spectra, which are more surface sensitive than Ga 3d and As 3d due to much higher binding energy. This diffusion process facilitates blue shift of the PL emission due to indium out-diffusion from the quantum well.

5.2. Crystalline BaO on GaAs(100) (paper 2)

This paper deals with improving the insulator/GaAs interface and therefore has a similar goal as paper 1. We demonstrate the growth of crystalline barium oxide on GaAs(100) at low temperatures, even at room temperature. The samples were studied using XPS, PL, STM and STS.

Two types of samples were prepared in UHV. One was reference sample without BaO where the GaAs surface was first cleaned from amorphous oxides and then an Al_2O_3 layer was grown on top of it using atomic layer deposition (ALD). For the other types we grew BaO on clean GaAs(100) surface by thermally evaporating Ba from a tantalum envelope while simultaneously raising oxygen pressure in the chamber. For PL measurements we then capped these samples with ALD grown Al_2O_3.

The initial experiment was to study the behavior of Ba atoms on clean GaAs surface with LEED and STM. The deposition of less than a monolayer of Ba produced a c(8×2) surface reconstruction even without post growth annealing. When the amount of Ba on the surface was increased to over 1 ML, Ba-nanolines appeared.

When the Ba deposition of 0.5 – 1.0 ML/min was done simultaneously with oxygen partial pressure of $1 – 10 \times 10^{-7}$ mbar it was possible to grow crystalline BaO films. These films are epitaxial and showed a (1×1) diffraction pattern after growth. Figure 22 shows both an STM image and a STS spectrum of such a film.
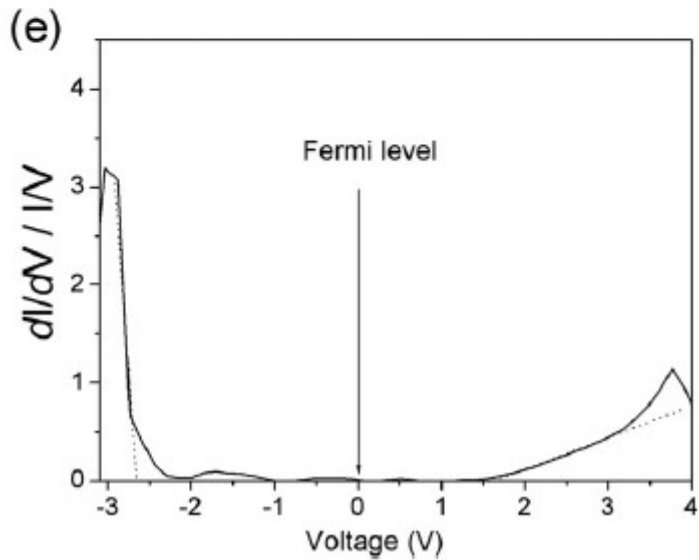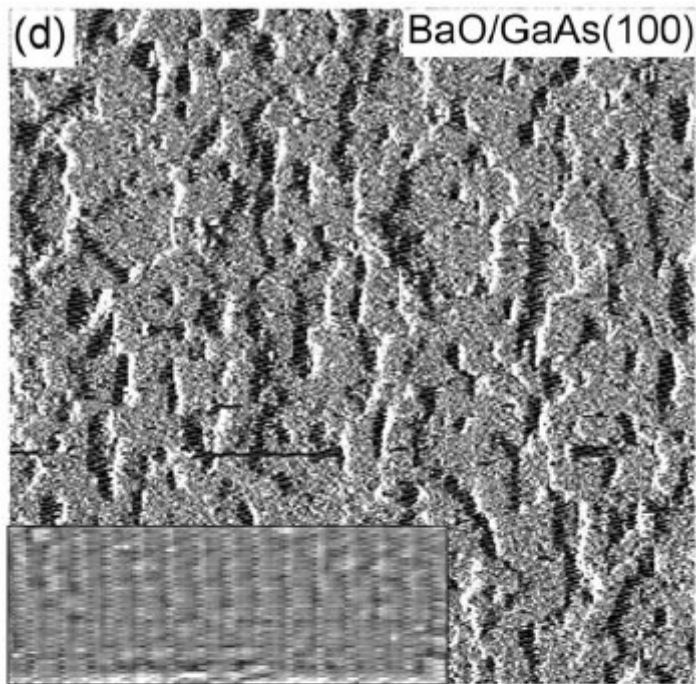
Figure 22. (d) STM and (e) STS of BaO on GaAs(100). The inset in (d) is a zoomed filled state image from the BaO surface. (e) is a differentiated STS curve measured from the BaO film surface.

To study the effect of BaO on interface defect density we made PL measurements. For these we had a Al_2O_3/GaAs reference sample and a Al_2O_3/BaO/GaAs sample. The PL spectra reveal that the interface defect density is lower in the sample containing the BaO layer. The junction tolerates RTA at 350 ºC – 550 ºC, but at 700 ºC a significant drop in PL intensity is seen. XPS measurements confirm that the BaO/GaAs interface contains Ga_2O, which is linked to improve the interface. XPS and PL spectra before RTA can be seen in Fig. 23. XPS spectra shown in Fig. 24 reveals that after 700 ºC some of the Ga atoms has diffused to the insulator and degraded the interface quality.
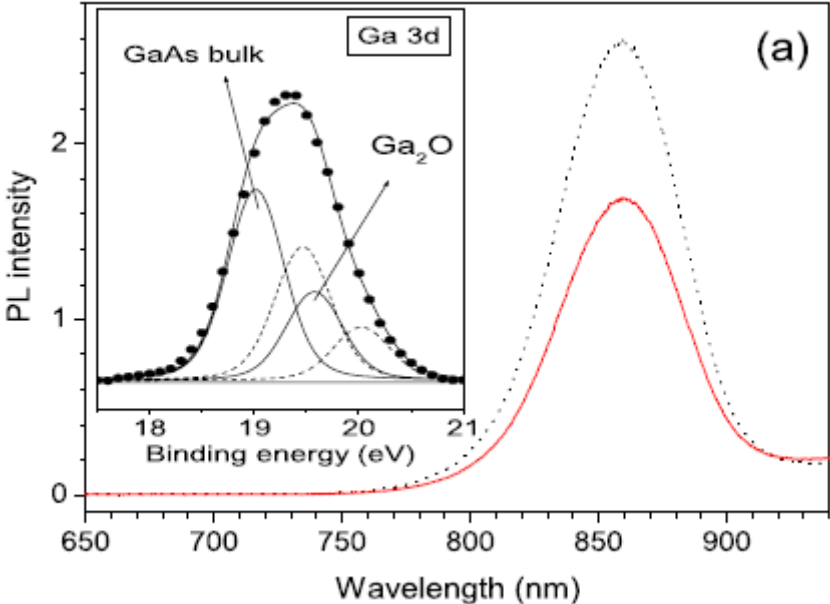

Figure 23. PL emissions of Al_2O_3/BaO/GaAs sample (dotted) and Al_2O_3/GaAs (solid). The inset shows Ga 3d spectrum from the Al_2O_3/BaO/GaAs sample.

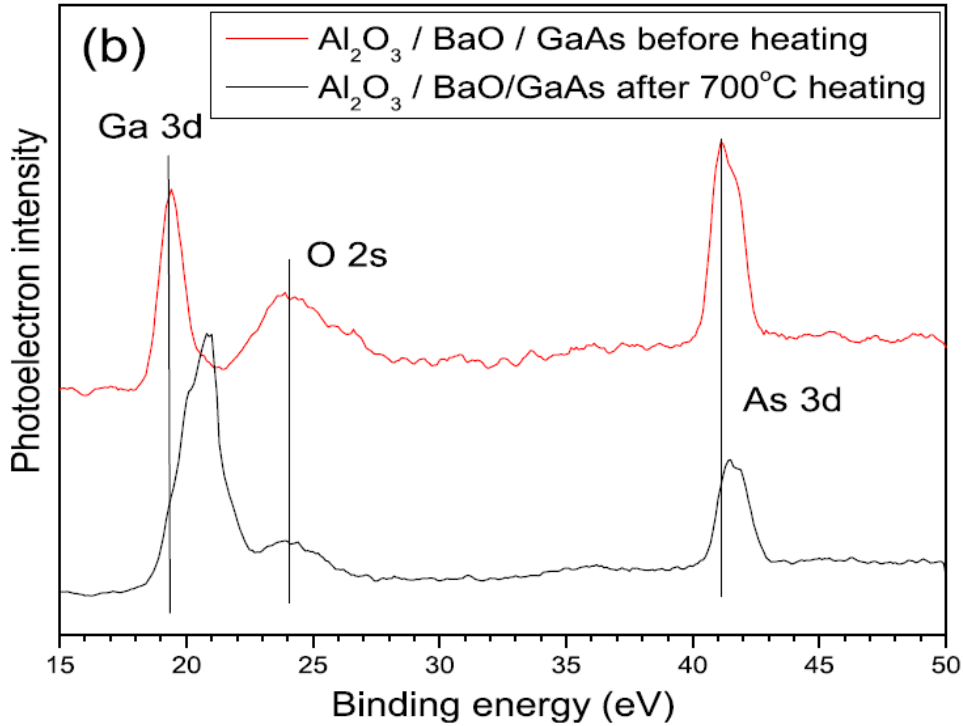*Figure 24. XPS-spectra from Al₂O₃/BaO/GaAs before (top) and after (bottom) 700 ºC RTA treatment. The Ga 3d peak is clearly shifted to higher binding energy after RTA.*

5.3. Polar InN(000-1) (paper 3)

InN has good potential in optoelectronics, but there are several difficulties which have to be overcome before the potential can be realized. One major hindrance is the formation of metallic In clusters and unintentional n-type conductivity in InN films during their synthesis. In this paper we demonstrate the formation of polar InN with surface Fermi level near the valence band maximum, as calculations have predicted. The synthesis and measurements were first done at beamline I4 in MAX-lab synchrotron radiation facility at University of Lund, Sweden and afterwards using a different substrate at University of Turku.

The InN on Si(111) samples were prepared as follows: The Si(111) sample surface was first cleaned in UHV. Then 2 – 3 monolayers of indium were deposited on top of it. The sample was then nitridated at 400 – 450 ºC and 10^{-4} mbar using thermally cracked nitrogen gas. Several In deposition/nitridation cycles were performed and the sample characterized after each cycle. This eventually produced flat InN islands such as in Fig. 25. To grow InN on GaN(0001) the procedure was similar as for Si substrate, but the nitridation gas was ammonia (NH$_3$). InN grew readily on GaN and the resulting films were much thicker than InN films on Si.

Figure 25. STM image of an InN island. The scale is 800 nm × 800 nm. The inset shows a zoomed in image taken from the top of a separate island.

SRPES spectra reveal major differences in the In 4d spectral line shape before and after nitridation. This is shown in Fig. 26 a). Valence band spectrum was also measured and along with STS measurements confirm the Fermi level position to be in the band gap near VBM, see Fig. 26 b). Our results indicate that a method to decrease the amount of unintentional electrons in InN is a process of alternating nitridation and In deposition.
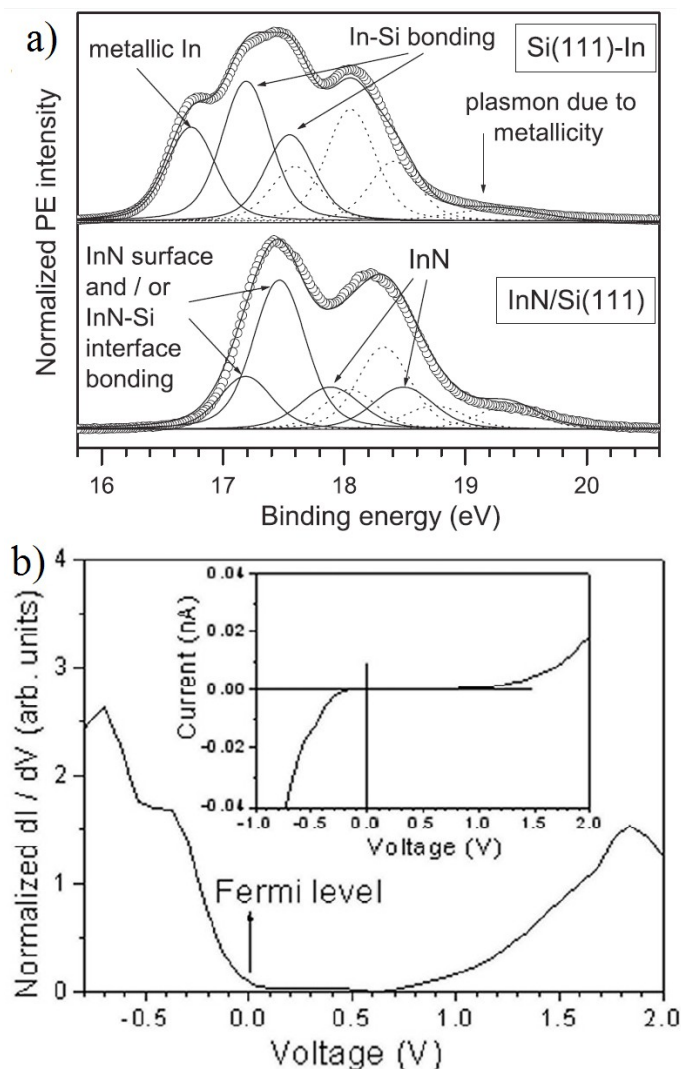

Figure 26. a) In 4d SRPES spectra from In covered Si substrate (top) and after nitridation and InN formation (bottom). b) STS spectrum from the top of an InN island showing the density of states. The inset shows the actual measurement.

The polarity of the InN films are concluded to be N-terminated InN(000-1). For InN on Si(111) this is supported by several facts: (1) only (1×1) LEED pattern was observed, (2) InN(0001) would grow via Si-N interface bonding, and (3) STM images revealed single step height to be 5.5 Å – 6.0 Å rather than 3 Å. For InN on GaN(0001) the results that support the conclusion are: (1) no trace of (√3×√3)-R30 or (2×2) LEED was observed, and (2) the growth temperature was 530 ºC – 580 ºC.

5.4. Photoluminescent GaAs nanoparticles (paper 4)

In this paper the fabrication and succesful surface passivation of GaAs nanoparticles are demonstrated. The conclusions are reached with the use of several complementary techniques, such as XPS, PL, transmission electron microscopy (TEM)[78], energy-dispersive X-ray spectroscopy (EDS)[43] and Raman spectroscopy[71].

Samples were fabricated using pulsed laser ablation in liquids.[79,80] Three different liquids were used: ethanol, de-ionized water and water solution containing ammonium sulphide $(NH_4)_2S$. The samples prepared in ethanol showed weak PL intensity. The samples made in de-ionized water showed no PL signal. The samples prepared in $(NH_4)_2S$ solution exhibited the best PL intensity. The optimal $(NH_4)_2S$ concentration in the solution was determined to be 1 mmol/l which gave an order of magnitude greater PL intensity than ethanol samples. With greater concentration the PL intensity began to diminish and redshift occurred. 120 seconds RTA at 375 ºC increased the PL intensity about an order of magnitude further. The RTA also induces redshift with PL peak wavelength increasing from 520 nm 550 nm.

TEM measurement reveal that the typical nanocrystal sizes are between 3 nm and 6 nm. The observed lattice constant was 0.555 nm which is smaller than the bulk value of 0.565 nm. TEM and EDS analyses show that the most stable particles have a GaAs core and the surface is a gallium rich compound with both sulfur and oxygen.

The XPS measurements of Ga $2p_{3/2}$ and As $2p_{3/2}$ before and after RTA are shown in Fig. 27. The oxygen components decrease with increasing sulfur content. RTA definitely changes the peak shape, especially for the 0.1 mmol samples, where heavy oxidation occurs. As oxidation is seen also with larger sulfur content, but it is known to not affect PL intensity. For 1 mmol sample RTA decreases the S-related component of Ga $2p_{3/2}$relatively.
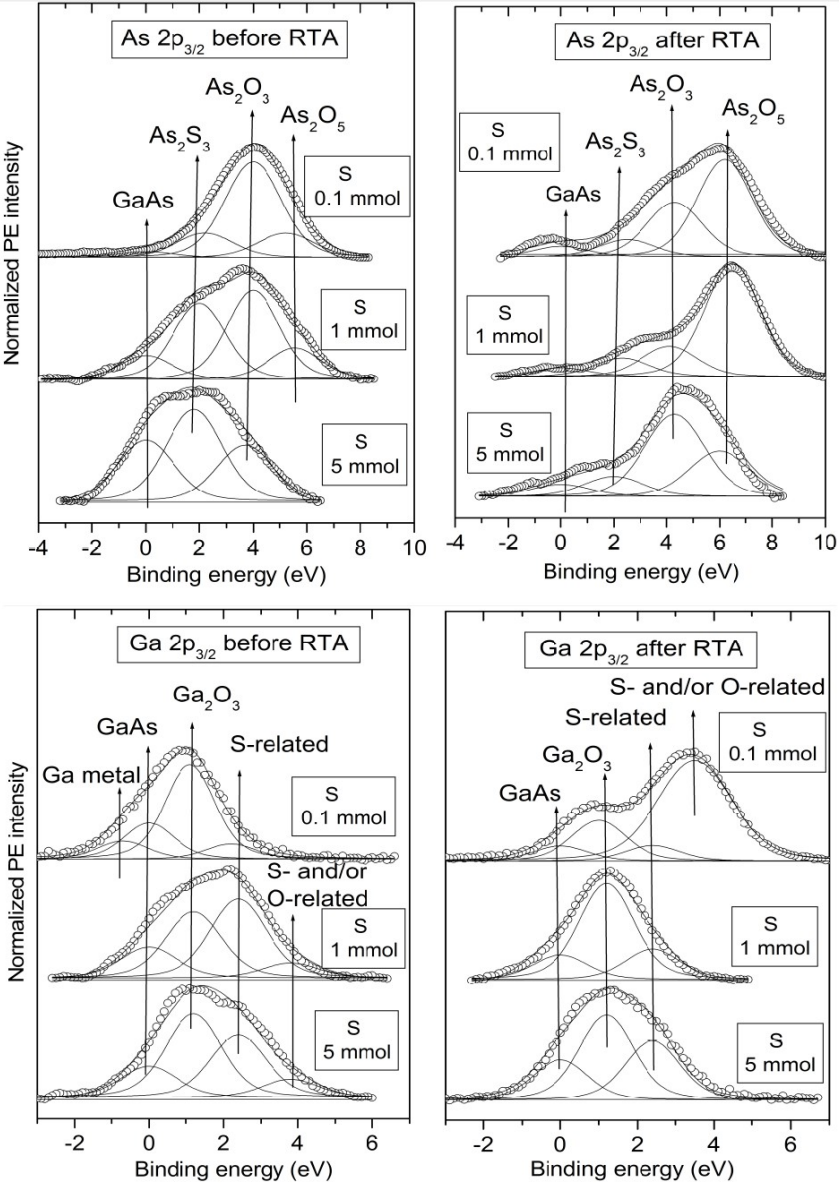

Figure 27. XPS spectra of As $2p_{3/2}$ and Ga $2p_{3/2}$ before and after RTA

The significant improvement of the photoluminescence of the samples passivated with $(NH_4)_2S$ is an indication of the succesful protective layer. The PL spectra were also unchanged for at least 6 months. Previous reports have shown GaAs wafer sulfur passivation to deteriorate within days. The extraordinary stability can be explained as follows: The nanocrystals in our samples have formed clusters and therefore the interfaces between nanocrystals have better protection. Also, the passivation layer is a compound of sulfur and oxygen which might be more stable than a passivation layer of sulfur alone.

5.5. Gallium interstitials in GaAsN (paper 5)

Ga(In)AsN dilute nitrides have attracted significant interest due to their unique properties.[81] They are especially important in optoelectronic point of view but even a small amount of nitrogen has been found to deteriorate the crystalline quality, but origin of such N-induced defects has remained unclear. This paper elucidates the formation energy of Ga interstitials in GaAsN by combining calculational results with SRPES and PL measurements. The calculations were performed using an *ab initio* density functional theory total-energy method within the local density approximation (LDA) by Docent Marko Punkkinen. SRPES measurements were done at MAX-lab beamline I311.

Calculational results demonstrate that the formation energy of Ga interstitial atom can be significantly decreased due to local effects within the defect complex. The model which is energetically the most favorable for a Ga interstitial atom in GaAsN is shown in Fig 28(a). In this model, the Ga interstitial is inside a Ga tetrahedron. Four nitrogen atoms stabilize the Ga interstitial by pulling out the Ga atoms in the tetrahedron surrounding the interstitial Ga atom. The formation energy is 1.46 eV smaller compared to model where the N atoms are not nearest neighbors of the Ga tetrahedron atoms, see Fig 28(b). The same mechanism was tested to apply to dilute nitrides of GaP and InAs, as well. The formation energy of Ga interstitials in GaAsN was noticed to be even lower at surfaces. These total-energy results are in very good agreement with the previous detection of Ga interstitials by measurement of optically detected magnetic resonance.
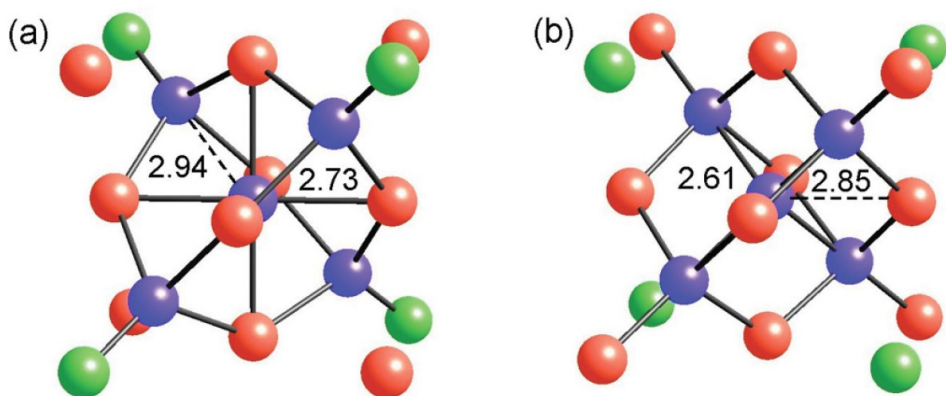
Figure 28. (a) The energetically most favorable model structure for a Ga interstitial atom in GaAsN. (b) Inequivalent structure for a Ga interstitial in GaAsN. Ga-As and Ga-Ga distances in Å around the Ga interstitial are also shown. Ga, As and N atoms are represented by blue, red and green spheres, respectively.

To destabilize the interstitial defect several dopant elements were considered. This dopant atom would stick to N atoms and therefore destabilize the Ga interstitial. Zr, Hf, Th and In incease the formation energy of the Ga interstitial atom the most if these atoms are the nearest neighbors of the Ga interstitial atom or not the nearest neighbors of the Ga interstitial atom but still the nearest neighbors of the N atoms.

To compare with the calculational results SRPES measurements were done with a variety of different photon energies. N 1s peak has three components. Their energy separation is small (total range about 0.5 eV), which allows to exclude many previously suggested atomic configurations such as N dimers. On the other hand, the N 1s results give a support to the presence of Ga interstitials, which is further supported by Ga 3d measurements. The Ga 3d spectra reveal a total of five components, one of which is attributed to Ga interstitial atoms, see Fig. 29 for both N 1s and Ga 3d spectra. The measured values for Ga core level shifts have a good correlation with calculational values for Ga model interstitial. PL measurement of the samples showed decrease of PL intensity with increasing nitrogen content showing evidence for increasing defect density.
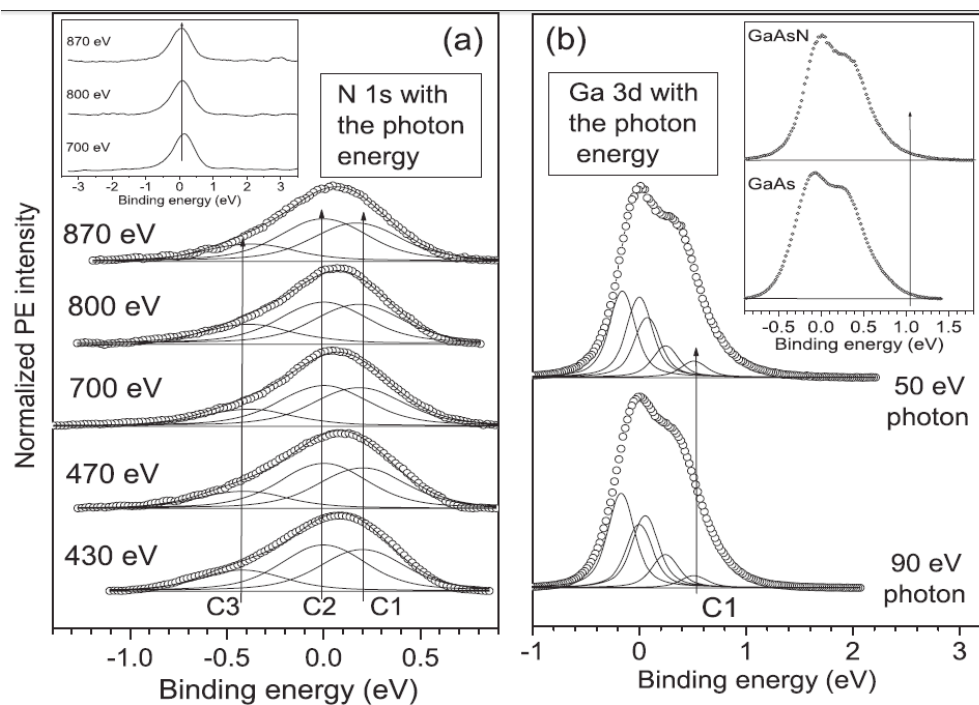
Figure 29. (a) N 1s and (b) Ga 3d SRPES spectra. The most surface sensitive spectrum for N1 s is taken with 470 eV photons. The 90 eV is more surface sensitive for Ga 3d. The inset in (a) shows larger scale spectra and the inset in (b) shows comparison between (2×4) pure GaAs and GaAsN films.

6. Conclusions

The theme connecting the papers in this thesis is the study of properties of defect-rich regions of III-V materials and the search for methods to reduce the defect density. The results can be divided to two categories: Insulator/semiconductor interface research (papers 1, 2, and 4), and research of pure III-V materials (papers 3 and 5). The main results are summarized below.

Insulator/GaAs interfaces were studied in papers 1 and 2. The low oxidation state of Ga (i.e., Ga_2O phase) has been found to be non-harmful; it does not increase defect density. Also, novel crystalline BaO layer enhanced PL intensity signalling

improvement of the interface. This effect has been found to remain up to 550 ºC post synthesis heating. Heating at higher temperatures was found to cause Ga diffusion into the the insulator film.

In paper 3 the formation of a novel material is demonstrated, polar InN(000-1) film. This film has the surface Fermi level near the VBM, a result predicted by calculations. A method to decrease the unintentional electron concentrations in InN films is to make cycles of In deposition and nitridation. In paper 4 the fabrication of photoluminescent and oxidized GaAs nanoparticles is demonstrated. These nanoparticles are stable and no deterioration of PL intensity was noticed for at least 6 months.

In paper 5 calculational results are combined with SRPES measurements. Ab initio calculations demonstrate that the formation of Ga interstitials in GaAsN is energetically favored, consisted with previous observation of Ga interstitials. The comparison of calculated CLS and SRPES measurements of GaAsN support the presence of Ga interstitials, and allows to exclude abundance of many previously suggested N-related defects. It is suggested that SRPES will be helpful in investigations of similar III-V materials if the surface effects can be efficiently removed, for example, by thin cap layers.

The use of complementary experimental techniques in addition to calculational studies is a powerful method to elucidate and investigate interfaces and novel materials alike. Especially XPS/SRPES combined with PL has proven its worth in the quest of clarifying the structure of buried interfaces.

References

[1] International Technology Roadmap for Semiconductors, 2013 edition, Process Integration, Devices, and Structures

[2] S. M. Sze and Kwok K. Ng, Physics of Semiconductor Devices, Third Edition, Wiley (2007)

[3] Fundamentals of III-V Semiconductor MOSFETs, edited by Serge Oktyabrsky and Peide D. Ye, Springer (2010)

[4] Yong-Bin Kim, Challenges for Nanoscale MOSFETs and Emerging Nanoelectronics, Transactions on Electrical and Electronic Materials **11,** 93 (2010)

[5] Toshihide Kikkawa, Kazukiyo Joshin and Masahito Kanamura, Fujitsu Sci. Tech. J. **48**, 40 (2012)

[6] I. Vurgaftman, J. R. Meyer and L. R. Ram-Mohan, Journal of Applied Physics **89**, 5815 (2001)

[7] Zongyou Yin and Xiaohong Tang, Solid-State Electronics **51**, 6 (2007)

[8] R. J. Singh, Solid State Physics, Dorling Kindersley (2012)

[9] Charles Kittel, Introduction to Solid State Physics, eighth edition, Wiley (2005)

[10] Handbook of Compound Semiconductors, edited by Paul H. Holloway and Gary E. McGuire, Noyes Publications

[11] G. H. Olsen, Journal of Crystal Growth **31**, 223 (1975)

[12] Ben, G. Streetman and Sanjay Kumar Banerjee, Solid State Electronic Devices, Pearson Education (2006)

[13] Marvin. L. Cohen and James R. Chelikowsky, Electronic Structure and Optical Properties of Semiconductors, Springer (1988)

[14] M. D. Pashley, Physical Review B **40**, 10481 (1989)

[15] Edmond Becquerel, Comptes Rendus **9**, 561 (1839)

[16] H. Hertz, Annalen der Physik **267**, 983 (1887)

[17] Zhen Zhang and John T. Yates Jr, Chemical Reviews **112**, 5520 (2012)

[18] Katsuaki Tanabe, Energies **2**, 504 (2009)

[19] D. L. Rode, Physical Review B **2**, 1012(1970)

[20] M. Passlack, R. Droopad, K. Rajagopalan, J. Abrokwah, P. Zucher and P. Fejes, High Mobility III-V MOSFET Technology, Compound Semiconductor Integrated Circuit Symposium, 2006

[21] I. G. Thayne, R. J. W. Hill, M. C. Holland, X. Li, H. Zhou, D. S. Macintyre, S. Thoms, K. Kalna, C. R. Stanley, A. Asenov, R. Droopad and M. Passlack, ECS

Transactions **19**, 275 (2009)

[22] Ioffe Institute, http://www.ioffe.ru/SVA/NSM/Semicond/index.html

[23] Liesbeth Venema, Nature **479**, 309 (2011)

[24] Charles B. Duke, Chemical Review **96**, 1237 (1996)

[25] Akihiro Ohtake, Jun Nakamura, Shiro Tsukamoto, Nobuyuki Koguchi and Akiko Natori, Physical Review Letters **89**, 206102 (2002)

[26] W. G. Schmidt, S. Mirbt and F. Bechstedt, Physical Review B **62**, 8087 (2000)

[27] K. Seiko, W. G. Schmidt and A. Ohtake, Physical Review B **73**, 035317 (2006)

[28] D. Paget, Y. Garreau, M. Sauvage, P. Chiaradia, R. Pinchaux and W. G. Schmidt, Physical Review B **64**, 161305 (2001)

[29] Robert F. Pierret, Semiconductor Device Fundamentals, Addison-Wesley (1996)

[30] Bhubaneswari Parida, S. Iniyan and Ranko Goic, Renewable and Sustainable Energy Reviews **15**, 1625 (2011)

[31] Martin A. Green, Keith Emery, Yoshihiro Hishikawa, Wilhelm Warta and Ewan D. Dunlop, Progress is Photovoltaics: Research and Applications **20**, 12 (2012)

[32] Hector Cotal, Chris Fetzer, Joseph Boisvert, Geoffrey Kinsey, Richard King, Peter Hebert, Hojun Yoon and Nasser Karam, Energy & Environmental Science **2**, 174 (2009)

[33] M. A. Green, Energy Policy **28**, 989 (2000)

[34] M. A. Green, Progress in Photovoltaics: Research and Applications **17**, 183 (2009)

[35] R. R. King, D. C. Law, J. T. Yen, M. Haddad, C. M. Fetzer, K. M. Edmondson, G. S. Kinsey, H. Yoon, M. Joshi, S. Mesropian, H. L. Cotal, D. D. Krut, J. H. Ermer and N. H. Karam, 21st European Photovoltaic Solar Energy Conference and Exhibition, Dresden, Germany, 2006, pp. 124-128

[36] Siddha Pimputkar, James S. Speck, Steven P. DenBaars and Shuji Nakamura, Nature Photonics **3**, 180 (2009)

[37] J. Bardeen and W. H. Brattain, Physical Review **74**, 230 (1948)

[38] Gordon Moore, Electronics **38**, (1965)

[39] Durga Misra, Hiroshi Iwai and Hei Wong, The Electrochemical Society *Interface*, (2005)

[40] C. L. Hinkle, M. Milojevic, B. Brennan, A. M. Sonnet, F. S. Aguirre-Tostado, G. J. Hughes, E. M. Vogel and R. M. Wallce, Applied Physics Letters **94**, 162101 (2009)

[41] D. S. L. Mui, Z. Wang and H. Morkoc, Thin Solid Films **231**, 107 (1993)

[42] Robert G. Wilson, F. A. Stevie and C. W. Magee, Secondary Ion Mass Spectrometry: A Practical Handbook for Depth Profiling and Bulk Impurity Analysis, Wiley (1989)

[43] Gernot Friedbacher and Henning Bubert, Surface and Thin Film Analysis: A Compendium of Principles, Instrumentation, and Applications, second edition (2011)

[44] H. R. Verma, Atomic and Nuclear Analytical Methods, Springer (2007)

[45] G. Binnig and H. Rohrer, Surface Science **126**, 236 (1983)

[46] M. Reason, H. A. McKay, W. Ye, S. Hansin, R. S. Goldman and V. Rotberg, Applied Physics Letters **85**, 1692 (2004)

[47] S. G. Spruytte, M. C. Larson, W. Wampler, C. W. Coldren, H. E. Petersen and J. S. Harris, Journal of Crystal Growth **227-228**, 506 (2001)

[48] C.-T. Kuo, S.C. Lin, K.K. Chang, H.-W. Shiu, L.-Y. Chang, C.-H. Chen, S.-J. Tang and S. Gwo, Applied Physics Letters **98**, 052101 (2011)

[49] A. Eisenhardt, M. Himmerlich and S. Krischok, Physica Status Solidi A **209**, 45 (2012)

[50] VASP web page, http://www.vasp.at/

[51] David S. Sholl and Janice A. Steckel, Density Functional Theory, Wiley (2009)

[52] G. Kresse and J. Hafner, Phys. Rev. B **47**, 558 (1993)

[53] G. Kresse and J. Hafner, Phys. Rev. B **49**, 14251 (1994)

[54] A. Einstein, Annalen der Physik **17**, 132 (1905)

[55] Official Web Site of the Nobel Prize,
http://www.nobelprize.org/nobel_prizes/physics/laureates/1921/

[56] John F. Moulder, William F. Stickle, Peter E. Sobol and Kenneth D. Bomben, Handbook of X-ray Photoelectron Spectroscopy, Perkin-Elmer (1992)

[57] M. P. Seah, Vacuum **34**, 463 (1984)

[58] Herbert Kromer, Nobel Lecture (2000)

[59] Timothy H. Gfroerer, Photoluminescence in Analysis of Surfaces and Interfaces in Encyclopedia of Analytical Chemistry, Wiley (2000)

[60] M. F. Koenig and J. T. Grant, Journal of Electron Spectroscopy and Related Phenomena **36**, 213 (1985)

[61] Handbook of Applied Solid State Spectroscopy, edited by D. R. Vij, Springer (2006)

[62] M. P. Seah and W. A. Dench, Surface and Interface Analysis **1**, 2 (1979)

[63] I. V. Veksler, Doklady Akad. Nauk SSSR **43**, 346 (1944)

[64] Edwin M. McMillan, Physical Review **68**, 143 (1945)

[65] MAX IV Rapport 5 (2006), available online at http://www.vr.se/download/18.61c03dad1180e26cb8780006182/MAXIV.Rapport5.2006.pdf

[66] Philip Willmott, An Introduction to Synchrotron Radiation, Wiley (2011)

[67] Joseph Larmor, Philosophical Transactions of the Royal Society of London A **190**, (1897)

[68] P. Schmüser, M. Dohlus, J. Rossbach and C. Behrens, Free-electron lasers in the ultraviolet and X-ray regime, second edition, Springer (2014)

[69] https://www.maxlab.lu.se/beamlines/I4

[70] https://www.maxlab.lu.se/node/26

[71] Semiconductor Research: Experimental Techniques, edited by Amalia Patanè and Naci Balkan, Springer (2012)

[72] C. J. Davisson, Bell System Technical journal **7**, 90 (1927)

[73] Handbook of Surface Science Volume 1: Physical Structure, edited by W. N. Unertl, Elsevier (1996)

[74] Official Web Site of the Nobel Prize, http://www.nobelprize.org/nobel_prizes/physics/laureates/1986/

[75] J. C. Vickerman, Surface Analysis: the Principal Techniques, Wiley (1997)

[76] Paul K. Hansma and Jerry Tersoff, Journal of Applied Physics **61**, R1 (1986)

[77] Scanning Tunneling Microscopy, edited by Joseph A. Stroscio and William J. Kaiser, Academic Press (1993)

[78] Brent Fultz and James M. Howe, Transmission Electron Microscopy and Diffractometry of Materials, third edition, Springer (2008)

[79] A. A. Lalayan, Applied Surface Science **248**, 209 (2005)

[80] R. A. Ganeev, M. Baba, A. I. Ryasnyansky, M. Suzuki and H. Kuroda, Applied Physics B **80**, 595 (2005)

[81] Physics and Applications of Dilute Nitrides, edited by I. A. Buyanova and W. M. Chen, Taylor & Francis (2004)